TU Delft

Delft University of Technology

Document Version
Final published version

Licence
CC BY-NC

Citation (APA)
Balakrishnan, S., & Stokkink, P. (2026). Role of topology and recovery strategies on multi-dimensional resilience of road networks. *International Journal of Disaster Risk Reduction*, *144*, Article 106366. https://doi.org/10.1016/j.ijdrr.2026.106366

Important note
To cite this publication, please use the final published version (if applicable).
Please check the document version above.

Copyright
In case the licence states “Dutch Copyright Act (Article 25fa)”, this publication was made available Green Open Access via the TU Delft Institutional Repository pursuant to Dutch Copyright Act (Article 25fa, the Taverne amendment). This provision does not affect copyright ownership.
Unless copyright is transferred by contract or statute, it remains with the copyright holder.

Sharing and reuse
Other than for strictly personal use, it is not permitted to download, forward or distribute the text or part of it, without the consent of the author(s) and/or copyright holder(s), unless the work is under an open content license such as Creative Commons.

Takedown policy
Please contact us and provide details if you believe this document breaches copyrights.
We will remove access to the work immediately and investigate your claim.

*This work is downloaded from Delft University of Technology.*

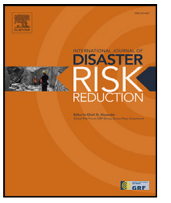
International Journal of Disaster Risk Reduction 144 (2026) 106366



Contents lists available at ScienceDirect

International Journal of Disaster Risk Reduction

journal homepage: www.elsevier.com/locate/ijdrr



# Role of topology and recovery strategies on multi-dimensional resilience of road networks☆

Srijith Balakrishnan *, Patrick Stokkink *

*Faculty of Technology, Policy and Management, Delft University of Technology, Jaffalaan 5, 2628 BX Delft, The Netherlands*

ARTICLE INFO

Dataset link: https://github.com/srijithbalakrishnan/transport_stresstesting

*Keywords:*
Topological metrics
Disaster resilience
Statistical analysis
Urban transport planning
Disruptions
Restoration

ABSTRACT

This paper examines how road network topology and post-disruption recovery strategies jointly shape recovery processes following disruptions. We develop a scalable stress-testing framework to simulate disruption scenarios and generate recovery data for road networks, which is subsequently analyzed with regression models to identify the effects of structural characteristics, recovery strategy, and disruption severity on multi-dimensional resilience. Using 224 real-world road networks, we assess their post-disruption recovery across five resilience dimensions: operational efficiency, accessibility, local redundancy, global connectivity, and spatial fairness. The results yield three key insights with significant implications on infrastructure design and management. First, road network resilience is fundamentally multidimensional: no single recovery strategy consistently performs best across all dimensions. Second, topological characteristics influence recovery outcomes. Third, strategy-based recovery provides limited benefits under minor disruptions but substantially accelerates recovery under severe damage. These findings highlight the need for policies that integrate robust and diverse network design with post-disaster recovery planning for resilience management.

## 1. Introduction

Transport networks are critical infrastructure systems that enable the movement of people, goods, and services. Yet, they are increasingly exposed to natural hazards, security threats, and infrastructure failures, among others. In the event of disasters, road networks are critical lifelines for communities. They provide access to hospitals, relief supply routes, and other emergency services. Their disruption can severely hinder recovery efforts, as seen during recent events such as the 2019–2020 Australian bush fires [1], the 2025 California wildfires [2], and the 2023 Northern India floods [3]. Collapsed bridges and damaged roads not only delay emergency response, but also trigger a wide range of cascading impacts, including travel delays, supply chain disruptions, inequitable access to essential services, and significant economic and societal costs [4,5]. These challenges, combined with increasing risks from climate-related and human-made hazards, have made resilience a priority in transport infrastructure planning and management.

Although resilience research in transportation has expanded rapidly over the past decade, much of this work has emphasized single-dimensional performance measures, such as efficiency or connectivity [6,7]. A few studies acknowledge the multidimensional nature of road network resilience; however, they primarily focus on multi-objective optimization of transport infrastructure recovery. In real-world contexts, however, recovery strategies based on predefined rules or goals are often preferred over optimization methods because of practical considerations and ease of implementation. A well-known example is the ‘eight-direction strategy’ of the East and

☆ This article is part of a Special issue entitled: ‘MSRRA-ERIC’ published in International Journal of Disaster Risk Reduction.

* Corresponding authors.
*E-mail addresses:* s.balakrishnan@tudelft.nl (S. Balakrishnan), p.s.a.stokkink@tudelft.nl (P. Stokkink).

https://doi.org/10.1016/j.ijdrr.2026.106366
Received 2 April 2026; Received in revised form 17 July 2026; Accepted 5 August 2026
Available online 24 August 2026
2212-4209/© 2026 The Authors. Published by Elsevier Ltd. This is an open access article under the CC BY-NC license (http://creativecommons.org/licenses/by-nc/4.0/).

## Nomenclature

### List of Notations

| | |
|---|---|
| $\alpha_{ij}$ | Adjacency indicator; $\alpha_{ij} = 1$ if an arc connects $v_i$ to $v_j$, and 0 otherwise |
| $\beta_{0,m}$, $\beta_{1,m}$ | Intercept and coefficient of disruption intensity, respectively |
| $\Delta(G(t))$ | Number of triangles in the underlying undirected representation of $G(t)$ (local redundancy) |
| $\delta_{r,m}$ | Coefficient of topological descriptor $x_r$ |
| $\epsilon$ | Small constant preventing division by zero in the proximity weights |
| $\eta_m$ | Linear predictor of the beta regression model for dimension $m$ (logit link) |
| $\gamma_{h,m}$ | Coefficient of the strategy indicator $\mathbb{I}(h)$ |
| $\lambda_{\max}$ | Largest (dominant) eigenvalue of the transpose of the weighted adjacency matrix $\mathbf{A}$ |
| $\mathbb{I}(h)$, $S$ | Indicator variable for recovery strategy $h$ and the set of non-reference strategies, respectively |
| $\mathbf{A}$, $A_{ji}$ | Weighted adjacency matrix and its entry for the directed arc $j \to i$ |
| $\mathbf{P}_m$ | Cumulative performance loss on dimension $m$ over the recovery trajectory (trapezoidal integration), $\mathbf{P}_m \in [0, 1]$ |
| $\mathcal{A}_r(t)$ | Accessibility of vertex $v_r$ at restoration step $t$ |
| $\mathcal{P}$ | Set of initial damage percentages considered in the experiments |
| $\mathrm{LCC}(G(t))$ | Number of vertices in the largest connected component of $G(t)$ (global connectivity) |
| $\mu_m$ | Expected value of the standardized performance metric for dimension $m$ |
| $\nu$ | Restoration batch size, expressed as a percentage of the total number of links restored per step |
| $\overline{\mathcal{A}}(t)$ | Mean accessibility across all vertices at restoration step $t$ |
| $\phi$ | Precision parameter of the beta regression model |
| $\psi_{h,m}$ | Coefficient of the interaction between strategy $h$ and disruption intensity |
| $\rho_i$ | Strength of vertex $v_i$, $\rho_i = \sum_{j \in V}(\sigma_{ij} + \sigma_{ji})$ |
| $\sigma_{ij}$ | Travel time of arc $(v_i, v_j)$; $\sigma_{ij} = \infty$ if $\alpha_{ij} = 0$ |
| $\sigma_{ij}(t)$ | Shortest-path travel time between $v_i$ and $v_j$ in $G(t)$ |
| $\sigma_{rs}$ | Travel time of the shortest route between vertices $v_r$ and $v_s$ |
| $\theta_{rs}$ | Number of shortest routes between vertices $v_r$ and $v_s$ |
| $\theta_{rs}(x)$ | Number of shortest routes between $v_r$ and $v_s$ passing through $x$, where $x$ is a vertex or an arc |
| $b$ | Distance-decay parameter of the proximity weights (set to 1.0 in this study) |
| $C_i$ | Closeness centrality of vertex $v_i$ in the undisrupted network, used as a proxy for the concentration of opportunities |
| $C_i^{\mathrm{EV}}$, $C_{ij}^{\mathrm{EV}}$ | Eigenvector centrality of vertex $v_i$ and of arc $(i, j)$, respectively |
| $C_{ij}^{\mathrm{B}}$ | Betweenness centrality of arc $(i, j)$ |
| $C_{ij}^{\mathrm{NN}}$ | Nearest-neighbor edge centrality of arc $(i, j)$ |
| $C_{ij}^{h}$ | Priority score of arc $(i, j)$ under strategy $h$ |
| $C_{v_i}^{\mathrm{C}}$, $C_{ij}^{\mathrm{C}}$ | Closeness centrality of vertex $v_i$ and of arc $(i, j)$, respectively |
| $C_{v_i}^{\mathrm{D}}$, $C_{ij}^{\mathrm{D}}$ | Degree centrality of vertex $v_i$ and of arc $(i, j)$, respectively |
| $d_{rs}$ | Euclidean distance between vertices $v_r$ and $v_s$ in the intact network |
| $G(t)$ | Partially restored network at restoration step $t$; $G(0)$ denotes the network immediately after disruption |
| $G = (V, A)$ | Directed graph representing a road network, with vertex set $V$ and arc set $A$ |
| $G_{\max}$ | Maximum attainable Gini coefficient ($G_{\max} = 1$) |
| $h$ | Index of a recovery strategy, $h \in H$ |
| $H = \{\mathrm{B}, \mathrm{D}, \mathrm{NN}, \mathrm{C}, \mathrm{EV}\}$ | Set of centrality-based recovery strategies (betweenness, degree, nearest-neighbor edge, closeness, eigenvector), complemented by a random baseline |
| $m$ | Index of a resilience dimension, $m \in \{\mathrm{Efficiency}, \mathrm{Accessibility}, \mathrm{Redundancy}, \mathrm{Connectivity}, \mathrm{Fairness}\}$ |
| $N$ | Number of random disruption realizations per network–damage–strategy combination |
| $P_m(t)$ | Normalized performance on dimension $m$ at restoration step $t$, $P_m(t) \in [0, 1]$ |
| $pct$ | Initial damage intensity, expressed as the percentage of disrupted links; $pct \in \mathcal{P}$ |
| $Q(t)$ | Far component of the spatial Gini decomposition of accessibility at restoration step $t$; $Q(0)$ denotes its value for the intact network |

| | |
|---|---|
| $R$, $x_r$ | Topological descriptor $r$ and the set of retained topological predictors, respectively |
| $t$ | Restoration step counter (dimensionless, sequential) |
| $t_0$, $t_r$ | Restoration steps corresponding to the occurrence of the disruption and to full recovery, respectively |
| $w_{rs}$ | Distance-based proximity weight between vertices $v_r$ and $v_s$ |

West Nippon Expressway Company in Japan, which prioritizes restoring eight key directional routes to ensure regional connectivity after disasters [8]. Yet, in such cases, recovery strategies that maximize efficiency may fail to guarantee equitable access, while those that improve connectedness may compromise overall system efficiency. The current literature does not provide clear evidence on the trade-offs among these competing performance objectives in strategy- or rule-based recovery planning. To address this gap, a scalable stress-testing framework and a large-scale test dataset encompassing diverse network topologies are needed.

Beyond these trade-offs, it is also essential to understand how resilience unfolds over time. Resilience operates at multiple stages: absorptive, restorative, and adaptive phases [9]. Absorptive capacity of networks is shaped by component robustness and network redundancy, which determine how much performance is lost during disruptions. Recovery, by contrast, depends on the prioritization of repairs and the sequencing and timing of interventions. Adaptive capacity is particularly relevant for transport systems facing evolving risks such as climate change, as it reflects the flexibility to adjust both absorptive and restorative functions under shifting conditions. While absorptive and restorative capacities are often studied separately, the interplay between these capacities in determining resilience outcomes is less explored. In the context of transport networks, research has shown how topology influences absorptive capabilities; however, the influence of network topology on restorative capacity in real-world settings is not yet well established. Investigating this relationship is critical for designing infrastructure systems that are both robust to shocks and capable of recovering rapidly when failures occur.

Based on the above considerations, this study develops a scalable framework for stress-testing road network resilience under multiple disruption scenarios and recovery strategies. Using a global dataset of 224 urban road networks extracted from OpenStreetMap, we evaluate recovery trajectories using five resilience dimensions, namely, operational efficiency, accessibility, local redundancy, global connectivity, and spatial fairness. Through large-scale simulation and regression analysis, we identify how disruption intensity, recovery strategy, and underlying network topology interact to shape resilience outcomes. The following are the specific objectives of the paper.

- To develop a computational stress-testing framework using OpenStreetMap data, designed for easy application to new cities, performance metrics, and recovery strategies without requiring additional inputs.
- Evaluate how topological features and heuristics-based recovery strategies interact and influence performance across multiple recovery objectives (multidimensional resilience), with the aim of providing guidelines for decision-makers and emergency managers.
- Examine the circumstances under which the topological characteristics of a network are associated with recovery, thereby providing large-scale simulation-based evidence for the influence of pre-disaster road network design on post-disaster recovery outcomes.

The remainder of the paper is organized as follows. Section 2 reviews the relevant literature. Section 3 outlines the methodological framework. Section 4 presents results for a diverse set of networks, including a statistical analysis of the relationship between topological features and recovery strategy performance. Section 5 concludes with a discussion of practical and policy implications.

## 2. Related work

### 2.1. Modeling resilience of road networks

Transport system resilience is a multi-stage characteristic that reflect both the capacity to withstand disruptions and the ability to recover functionality afterward. While vulnerability, reliability, and risk each provide useful but partial perspectives, resilience uniquely captures the system's trajectory through disruption and recovery phases [10,11]. Building on early conceptualizations from ecology, [12] proposed the widely adopted 4R's framework (robustness, redundancy, resourcefulness, and rapidity) for socio-technical systems, which has since been extensively applied in transport resilience studies. In this framework, robustness and redundancy shape system performance during disruption, while resourcefulness and rapidity govern the effectiveness and speed of recovery. Similarly, [10] introduced one of the first transport-specific frameworks for resilience analysis, identifying ten interrelated dimensions including redundancy, efficiency, adaptability, and the ability to recover quickly. In several studies, especially among the network architecture community, resilience and robustness are interchangeably used [13,14]. However, in this study, we adopt the terminology from [12] 4R's framework.

Several studies converge on the view that resilience can be understood as a combination of absorptive and restorative capacities [9]. Absorptive capacity refers to the ability of a system to maintain critical functionality during disruptions, while restorative

capacity encompasses the resources and time required to restore service levels afterward. In transport networks, absorptive capacity is shaped by inherent structural properties [15], such as density, redundancy, and modularity, whereas restorative capacity is influenced by the ability to mobilize resources and implement dynamic strategies for scheduling repairs and reallocating flows [16,17]. Together, these phases define resilience as an evolving trajectory that spans disruption and recovery stages, rather than a single scalar indicator.

To operationalize these conceptual frameworks, a wide range of resilience metrics has been proposed, which can be grouped into three categories: topological or structural, attribute-based, and performance-based [18]. Topological measures (e.g., centrality, clustering) capture structural properties but neglect operational dynamics. Attribute-based metrics often quantify specific resilience properties, such as recovery speed or efficiency. Performance-based metrics assess functionality over time, often by measuring cumulative losses (e.g., area under the resilience curve). While topological metrics are computationally efficient and widely used for heuristic recovery planning, performance-based measures are essential for capturing user-level impacts such as accessibility, equity, or delays [19,20]. However, for stress-testing a large number of transport networks and develop generalized policy insights into network design, topological metrics have been widely used in the literature [7].

Although earlier efforts focused on one aspect of resilience, recent studies increasingly emphasize the multidimensional nature of recovery decisions in road infrastructure [4,21] and the wider transport and logistics domains [22,23]. Transport systems are socio-technical systems, and post-disaster recovery planning involves multiple, often conflicting objectives [24]. In this context, planners must balance operational efficiency [25] against equitable access [26,27], connectivity [28], feasibility and cost [29], and other practical constraints. For example, a strategy that prioritizes major highways may maximize traffic flow but leave peripheral communities isolated or exceed budget limits. However, resilience is still commonly measured using a single time-varying indicator, typically summarized as the area under the performance curve. Such scalar measures capture one dimension of recovery but miss how accessibility or equity is restored for different user groups or regions. To illustrate the multidimensional aspect of resilience, Fig. 1 shows how the resilience curves depicting road network recovery can be sensitive to the choice of performance metric. In summary, a recovery that appears effective by one network-wide indicator may perform poorly on another objective. Therefore, a multidimensional approach is required to evaluate recovery strategies and provide holistic insights to decision-makers.

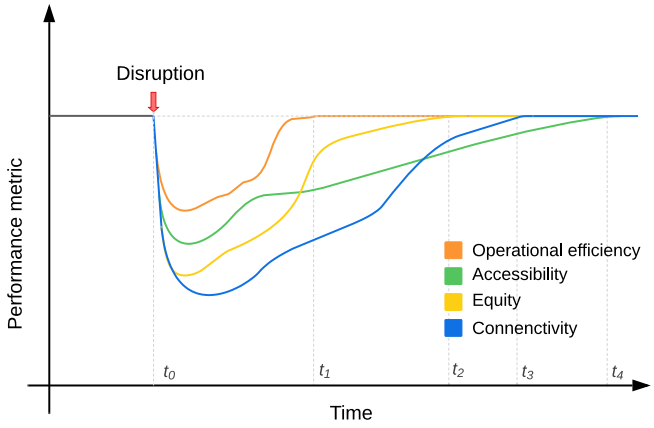



**Fig. 1.** Illustrative example of multi-dimensional impacts of road recovery strategies. Network-level recovery can assume very different trajectories based on the metric that is used to measure it. This underlines the need for integrated recovery strategies that balance relevant transport objectives.

### *2.2. Recovery planning and prioritization methods*

As a crucial element of resilience, post-disaster recovery planning has received considerable attention in the literature. Recovery of networks is a dynamic problem where the sequence of restoring damaged links must be determined under resource and time constraints [30]. Because not all components can be repaired simultaneously, prioritizing which links to recover first has significant implications for how quickly and equitably the system regains functionality. This problem is inherently multi-objective: strategies that maximize efficiency may neglect accessibility for peripheral communities, while those prioritizing equity may impose longer delays or higher costs. In the literature, three types of recovery planning methods are identified: graph-based heuristics, network optimization approaches, and simulation-based approaches.

Graph-theoretic models rank nodes or links by importance using network indices and then guide repair sequencing. Studies show that networks with many high-degree or high-centrality nodes are especially vulnerable, and prioritizing their repair can restore flow more quickly than random strategies. Studies show that in infrastructure systems, such as transportation networks, water distributions systems and power systems, simple topology-based heuristics often outperform unguided rebuilding. For instance, [11] showed that topological heuristics can reduce resilience losses by 40%–50% compared to random recovery. More recent work extends this idea by combining centrality with operational indicators to define hybrid heuristics that balance structural efficiency with flow-based measures, often producing superior recovery outcomes [31]. Other studies propose network-science–inspired heuristics (e.g., Cent-Restore) that explicitly incorporate service network needs during restoration [32].

A large body of work formulates recovery planning as optimization problems, often bi-level or multi-objective, where the lower level computes flows and the upper level identifies optimal repair sequences. For example, [31] and [33] developed bi-level models balancing unmet demand and travel time, solved using network design heuristics. Metaheuristics such as discrete particle swarm optimization [34] and genetic algorithms [35] improve scalability. Multi-objective formulations are increasingly common: [21] showed how outcomes vary depending on user groups emphasized, while [36] integrated risk under uncertainty into restoration planning.

Simulation-based approaches are also widely used to capture uncertainty and recovery dynamics. Monte Carlo–based frameworks test strategies under stochastic hazards, particularly in rural or geohazard-prone regions [37]. Multi-agent and agent-based simulations integrate social, economic, and political dimensions into recovery, showing promise for community-sensitive planning. Recent studies highlight the potential of reinforcement learning and deep reinforcement learning to optimize sequencing under complex, uncertain conditions, accommodating multiple crews and heterogeneous objectives [38,39]. Scenario-based stress testing has also been applied to evaluate novel recovery techniques (e.g., accelerated bridge construction) in reducing downtime and indirect losses [7,40].

Comparisons across these categories reveal trade-offs between scalability and realism. Graph-based strategies are fast and transferable but abstract from demand and user-level impacts. Optimization models capture flows and trade-offs between efficiency, cost, and accessibility more accurately but are computationally intensive and case-specific. Simulation approaches best address uncertainty and heterogeneous objectives, but remain data-intensive and less generalizable.

### 2.3. Relationship between road network topology and recovery

Because network topology influences both initial damage and rerouting possibilities, it likely shapes the absorptive and restorative capacities of networks. Prior research hints at the existence of a causal relationship, tying resilience to network density, key nodes, and path redundancy [41]. Yet, systematic evidence on how topology drives multidimensional recovery outcomes remains sparse. On the one hand, densely interconnected grids facilitate rapid traffic rerouting, boosting efficiency and equitable access. On the other hand, sparse, tree-like structures risk cascading failures and prolonged reconnection. Quantifying these dynamics is essential: it equips planners to anticipate performance from specific layouts before disasters unfold.

This underscores the value of integrated approaches, such as coupled resilience planning, which calls for joint resource allocation across absorptive and restorative dimensions [29,42]. Although the interaction between the two resilience capacities is underexplored, structural features of transport networks clearly affect routine operations and disruption responses. Advancing this line of research, [7] analyzed the association between topological characteristics on recoverability in 42 urban metro networks across the world. Yet, the multidimensional nature of resilience was overlooked. While many studies leverage multiple resilience metrics to optimize recovery sequences, evidence on the influence of network topology on multidimensional resilience in realistic road networks is still limited.

Network resilience and robustness are commonly analyzed through topological metrics. Applications span social networks [43,44], biological networks [45,46], economic networks [47,48], and transport networks. Within transportation, centrality measures have been applied to air transport [49], metro networks [50], and road networks [51]. Reviews by Das et al. [52]; Landherr et al. [53] provide comparisons across centrality measures, while [54] focuses specifically on transportation networks. Across these studies, a common pattern emerges: most rely on a narrow set of centrality metrics. [54] identify 17 measures commonly used, but reviews by Landherr et al. [53] and Das et al. [52] show that only a handful of measures dominate applications. Centrality captures topological importance but not operational aspects such as flows or accessibility. Its popularity stems from computational efficiency and limited data requirements, making it valuable for design insights, but needs to be corroborated with performance-based metrics for operational insights.

### 2.4. Gaps in the literature

Despite significant advances in transport network resilience, several critical gaps remain, particularly in the context of multidimensional recovery planning and the association between network topology and recovery outcomes. Many existing studies focus on single-dimensional resilience metrics, such as efficiency or connectivity, often overlooking the complex trade-offs between competing transport objectives, such as equity, accessibility, connectivity, etc.

Strategies that optimize recovery for efficiency may not ensure (or worse, deteriorate) equity, while those that improve connectivity may compromise accessibility. Although some work has explored multi-objective optimization frameworks, these are typically theoretical or limited to specific scenarios, with limited validation of their practical applicability in real-world recovery planning. This gap is particularly pronounced in the context of rule- or strategy-based recovery, where predefined priorities are often adopted without rigorous analysis of their unintended consequences on other system-wide impacts.

In addition, the association between absorptive and restorative capacities, which are key components of transport network resilience, remains underexplored in real-world network settings. While absorptive capacity is frequently linked to network topology, restorative capacity has been mostly tied to optimal recovery and resource mobilization, with limited attention to how topological features shape recovery dynamics over time.

Finally, to address the above gaps quantitatively, data-driven frameworks for stress-testing resilience across diverse network topologies and recovery strategies leveraging open-source transport network data are required. While simulation-based approaches and optimization models have advanced, they often require extensive computational resources or case-specific data, limiting their applicability to develop generalized insights on the above gaps.

## 3. Methodology

The methodological framework of this study is summarized in Fig. 2. We begin by sampling road networks from [55] randomly across all geographic regions. Each network is converted into an abstract graph representation using the `igraph` package in Python [56], in which intersections are modeled as nodes and road segments as edges. This abstraction enables the use of graph-theoretic measures to describe structural and topological properties that may influence recovery dynamics. Disruptions are simulated by applying a random edge failure strategy, where an incremental percentage of edges is removed from the network each time. This procedure generates a disrupted network that reflects the stochastic nature of real-world events such as accidents, hazards, or attacks, but under varying levels of intensity. To model recovery, we define six strategies for restoring failed edges (road segments): degree centrality, edge betweenness centrality, nearest neighbor edge centrality, eigenvector centrality, closeness centrality, and a random baseline strategy. These strategies reflect alternative principles for prioritization, ranging from targeting highly connected nodes to restoring globally central links.

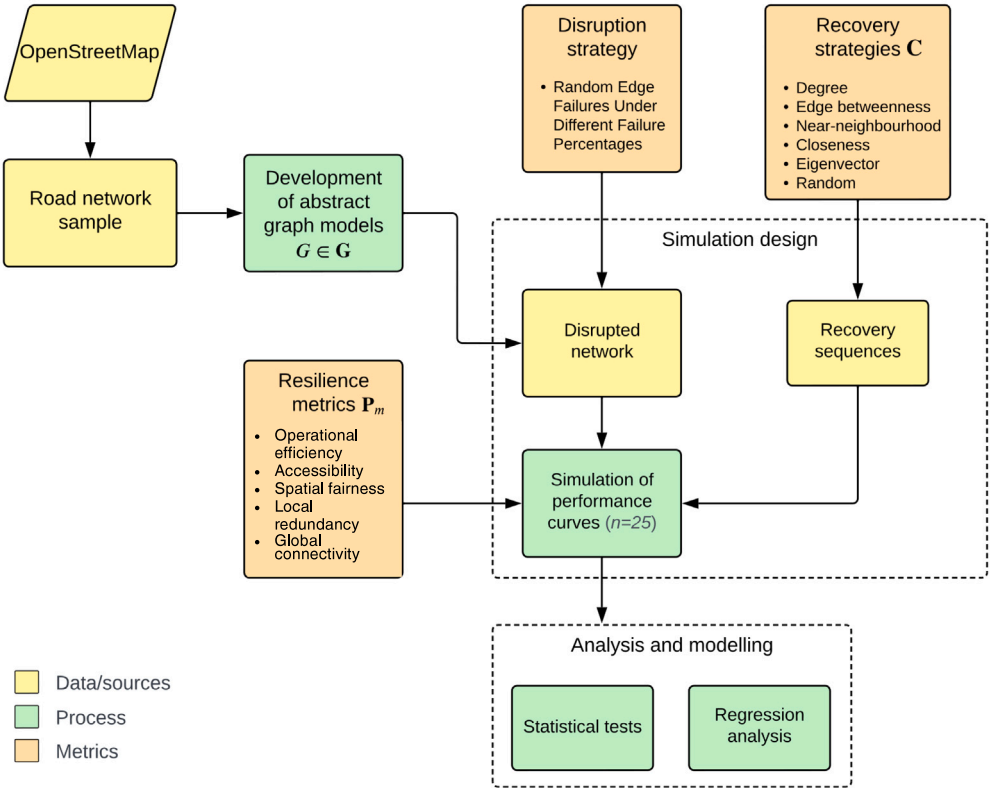



**Fig. 2.** Study methodology.

Effectiveness of recovery is measured using resilience metrics derived from five operational measures: (a) operational efficiency, (b) accessibility, (c) local redundancy, (d) global connectivity, and (e) spatial fairness. For each strategy, a recovery sequence is generated, and performance metrics are computed at each restoration step. The results are aggregated into performance curves for every resilience metric.

The simulated dataset is then used to perform statistical analyses and modeling. Beta regression models are developed to examine resilience outcomes (cumulative impact throughout the recovery process expressed as a fraction) as a function of network topology, disruption intensity, and recovery strategy. The statistical models allow us to unravel the influence of structural characteristics and recovery strategies, and to identify conditions under which specific strategies are most effective with respect to a specific resilience dimension.

### 3.1. Mathematical formulation

Each road network is represented as a directed graph $G = (V, A)$, in which the vertex set $V = \{v_1, \ldots, v_N\}$ corresponds to road junctions and the arc set $A$ corresponds to directed road segments. Directed arcs are used to allow for the incorporation of one-way streets. In the case of two-way streets, two separate arcs are introduced for each direction. We define $\alpha_{ij} = 1$ if vertices $v_i$ and $v_j$ are directly connected by an arc, and $\alpha_{ij} = 0$ otherwise. As we consider a directed graph $\alpha_{ij}$ does not need to be equal to $\alpha_{ji}$.

Accordingly, the arc set is defined as $A = \{(v_i, v_j) \mid v_i, v_j \in V \text{ and } \alpha_{ij} = 1\}$. We define $\sigma_{ij}$ as the travel time of arc $(v_i, v_j)$, where $\sigma_{ij} = \infty$ if $\alpha_{ij} = 0$. This also allows us to define $\sigma_{rs}$ as the travel time of the shortest route between $v_r$ and $v_s$ and $\theta_{rs}$ as the number of shortest routes between $v_r$ and $v_s$. Then, let $\theta_{rs}(x)$ denote the number of shortest routes between vertices $v_r$ and $v_s$ that pass through $x$, where $x$ may be either a vertex $v \in V$ or an arc $a \in A$. The topological metrics used as heuristics for post-disruption recovery sequence determination are defined as $C_{ij}^h$, for the arc $(i, j)$, respectively, where $h$ denotes the strategy ($C_{ij}^h \in \mathbf{C}$). The recovery strategies considered are denoted by $H = \{\text{B, D, NN, C, EV}\}$, each of which is described in detail in Section 3.2. In addition to the above strategies, a random recovery strategy was also considered as a baseline.

### 3.2. Recovery strategies

As previously mentioned, the recovery strategies $h \in H$ considered in this paper are based on centrality metrics. Link travel times, computed from open-source speed data, are further incorporated to identify shortest paths, while graph-based measures are employed to approximate demand and the relative importance of network components. Centrality-based recovery approaches have been extensively adopted in both academic and applied contexts, owing to their low computational complexity and straightforward implementation [57,58]. For every damaged arc $(i, j)$, we calculate a centrality metric denoted as $C_{ij}^h$, which serves as its priority score. The disrupted arcs are then ranked in descending order based on these scores, and recovery actions are scheduled and carried out in the simulations according to this ranking. In this study, we consider five centrality measures and a random sequencing strategy that are frequently used in the literature for guiding recovery decisions in transport infrastructure. The definitions of these centrality metrics are presented in the following part of this section.

#### 3.2.1. Betweenness centrality

Betweenness centrality quantifies the extent to which a vertex or arc lies on shortest paths connecting other components of the network [59]. Using the graph notation introduced earlier, the betweenness centrality of an arc $(i, j) \in A$, denoted $C_{ij}^{\mathrm{B}}$, is given by:

$$C_{ij}^{\mathrm{B}} = \sum_{r,s \in V, r \neq s, \sigma_{rs} > 0} \frac{\theta_{rs}(i,j)}{\theta_{rs}} \tag{1}$$

where $\theta_{rs}$ represents the total number of shortest paths between vertices $r$ and $s$, computed using link travel times $\sigma_{ij}$ as weights, and $\theta_{rs}(i, j)$ denotes the subset of those paths that traverse arc $(i, j)$.

#### 3.2.2. Degree centrality

Degree centrality captures local importance by counting the number of connections associated with a vertex or arc. In directed networks, vertex degree is decomposed into incoming and outgoing components. For a vertex $i$, the total degree centrality $C_{v_i}^{\mathrm{D}}$ is defined as the sum of its incoming and outgoing arcs:

$$C_{v_i}^{\mathrm{D}} = \sum_{k \in V, (i,k) \in A} \alpha_{ik} + \sum_{k \in V, (k,i) \in A} \alpha_{ki} \tag{2}$$

where $\alpha_{ik}$ and $\alpha_{ki}$ are indicator variables denoting the presence of arcs $(i, k)$ and $(k, i)$, respectively. The degree centrality of an arc $(i, j)$ is then computed as the product of the degree centralities of its incident vertices:

$$C_{ij}^{\mathrm{D}} = C_{v_i}^{\mathrm{D}} \cdot C_{v_j}^{\mathrm{D}} \tag{3}$$

#### 3.2.3. Nearest-neighbor edge centrality

Nearest-neighbor edge centrality is a local edge importance measure [60]. Because it relies primarily on local connectivity information, it offers computational advantages over global metrics and may be well-suited for time-critical recovery decisions. For an arc $(i, j)$, the nearest-neighbor edge centrality can be mathematically expressed as:

$$C_{ij}^{\mathrm{NN}} = \sigma_{ij} \left( \frac{\rho_i + \rho_j - 2\,\sigma_{ij}}{1 + |\rho_i - \rho_j|} \right) \tag{4}$$

where $\rho_i$ denotes the strength of vertex $i$, given by $\rho_i = \sum_{j \in V} (\sigma_{ij} + \sigma_{ji})$, and $\sigma_{ij}$ is the travel time associated with arc $(i, j)$.

This metric does not explicitly account for arc directionality and is limited in its ability to represent long-range structural dependencies within the network.

#### 3.2.4. Closeness centrality

Closeness centrality reflects how close a network component is to all others in terms of shortest-path distances. An arc is considered more central when it is embedded in generally shorter paths to the rest of the network. For an arc $(i, j)$, closeness centrality is computed as:

$$C_{ij}^{\mathrm{C}} = \frac{|A| - 1}{C_{v_i}^{\mathrm{C}} + C_{v_j}^{\mathrm{C}}} C_{v_i}^{\mathrm{C}} C_{v_j}^{\mathrm{C}}, \qquad C_{v_i}^{\mathrm{C}} = \frac{|V| - 1}{\sum_{k \in V} \sigma_{ki}} \tag{5}$$

where $\sigma_{ki}$ represents the shortest-path travel time from vertex $k$ to vertex $i$, calculated using travel times as edge weights, and $|V|$ denotes the total number of vertices. $C_{v_i}^{\mathrm{C}}$ is set to zero if vertex $i$ is not connected to any other vertices. Similarly, if $C_{v_i}^{\mathrm{C}} + C_{v_j}^{\mathrm{C}} = 0$, the arc-level closeness centrality $C_{ij}^{\mathrm{C}}$ is defined as zero.

#### 3.2.5. Eigenvector centrality

Eigenvector centrality assigns importance to nodes based on the importance of their neighboring nodes, such that connections to highly central nodes increase a node's score [61,62].

Let $\lambda_{\max}$ denote the largest (dominant) eigenvalue of the transpose of the weighted adjacency matrix $\mathbf{A}$, where $A_{ji}$ is the weight of the directed arc $j \to i$ (or 0 if no such arc exists). The node eigenvector centrality $C_i^{\mathrm{EV}}$ of node $i$ is obtained by solving the following system:

$$C_i^{\mathrm{EV}} = \frac{1}{\lambda_{\max}} \sum_{j \in V} A_{ji}\, C_j^{\mathrm{EV}} \tag{6}$$

To derive an edge importance score $C_{ij}^{\mathrm{EV}}$ for each arc $(i, j) \in A$, we find the arithmetic mean of the eigenvector centralities of its source vertex $i$ and target vertex $j$:

$$C_{ij}^{\mathrm{EV}} = \frac{C_i^{\mathrm{EV}} + C_j^{\mathrm{EV}}}{2} \tag{7}$$

This proxy assigns higher importance to arcs that connect (or are incident to) two highly central nodes.

### 3.3. Resilience metrics

The main objective of the study is to investigate the recovery of transport networks through a multi-dimensional approach. Specifically, we look at five dimensions of transport network recovery: operational efficiency, accessibility, local redundancy, global connectivity, and spatial fairness. We use network-level aggregate indicators for evaluating the recovery of networks under various strategies. To compare the recovery across networks, every metric is transformed to a fraction of the performance of the undisrupted network, resulting in all metrics being measured on a [0,1] scale. The resilience metrics $\mathbf{P}_m$ where:

$$m \in \{\text{Efficiency, Accessibility, Redundancy, Connectivity, Fairness}\}, \tag{8}$$

are used to evaluate cumulative performance loss under each recovery strategy, and are computed using the trapezoidal method as follows.

$$\mathbf{P}_m = \frac{\int_{t_0}^{t_r} \left(1 - P_m(t)\right) dt}{(t_r - t_0)} = \frac{\sum_{t=t_0}^{t_r - \Delta t} \left(1 - \frac{[P_m(t_i) + P_m(t_{i+1})]}{2}\right) \Delta t}{(t_r - t_0)}; \quad 0 \le \mathbf{P}_m \le 1, \tag{9}$$

where $P_m(t)$ is the performance based on resilience dimension $m$ at restoration step $t$. Throughout this study, $t$ denotes discrete restoration steps (simulation time) rather than physical time: at each step, a fixed batch of damaged links is restored, and network performance is re-evaluated. The recovery trajectories and the resilience metrics $P_m$ are therefore dimensionless and sequential, describing performance as a function of restoration progress rather than of elapsed clock time. Mapping restoration steps to real-world durations would require assumptions on repair times and crew capacity, which lie outside the hazard-agnostic scope of this framework.

The performance is measured between $t_0$ and $t_r$, where $t_0$ denotes the restoration step immediately after the disruption and $t_r$ the restoration step at which the network is fully recovered. Let $G$ be the undisrupted network and $G(0)$ be the network immediately after disruption. We also use $G(t) : t \ge 0$ denote the network at any timestep $t$ after the disruption, such that $\sigma_{ij}(t)$ denotes the shortest path length between vertices $v_i$ and $v_j$ in graph $G(t)$.

#### 3.3.1. Operational efficiency

Operational efficiency captures the ease with which travelers can move from their origins to destinations within the network. We operationalize this concept using the global network efficiency, defined as the inverse of the shortest-path travel times between all ordered node pairs. The normalized network efficiency at timestep $t$ is defined as:

$$P_{\text{Efficiency}}(t) = \frac{\text{Efficiency}(G(t))}{\text{Efficiency}(G)}. \tag{10}$$

$$\text{Efficiency}(G(t)) = \frac{1}{|V|(|V| - 1)} \sum_{r=1}^{|V|} \sum_{\substack{s=1 \\ s \ne r}}^{|V|} \frac{1}{\sigma_{rs}(t)}, \qquad \sigma_{rs}(t) < \infty, \tag{11}$$

where $\sigma_{rs}(t)$ denotes the shortest-path travel time between nodes $v_r$ and $v_s$ at timestep $t$. Node pairs that are disconnected (i.e., $\sigma_{rs}(t) = \infty$) contribute zero to the summation. The efficiency of the disrupted network is normalized by the efficiency of the undisturbed network, such that $P_{\text{Efficiency}} = 1$ for the intact network.

In this study, operational efficiency is computed using purely topological information and does not account for origin–destination demands or traffic flows, although such weighting could be incorporated in future extensions. Lower values of $P_{\text{Efficiency}}$ indicate reduced resilience with respect to operational performance.

### 3.3.2. Accessibility

Accessibility reflects the ease with which locations in the network can be reached from one another. We quantify accessibility using a closeness-centrality–based measure that weights travel times by the relative importance of destination nodes. For a vertex $v_r$, its accessibility at timestep $t$ is defined as

$$A_r(t) = \sum_{\substack{i=1 \\ i \neq r}}^{|V|} \frac{C_i^C}{\sigma_{ri}(t)}; \quad \sigma_{ri}(t) < \infty, \tag{12}$$

where $C_i^C$ represents the closeness centrality of vertex $v_i$ computed on the undisrupted network $G$. The closeness centrality of the undisrupted network serves as a proxy for the concentration of social and economic opportunities at node $i$, under the assumption that more central nodes tend to host higher levels of activity (e.g., central business districts). This relationship between street-network centrality and the density of economic activity is well documented empirically [49,63] and enables consistent accessibility assessment across cities for which harmonized population and land-use data are unavailable. The proxy nevertheless abstracts from actual travel demand, population density, and socio-economic composition, and may bias accessibility estimates towards the geometric center of the network in cities with polycentric or peripheral activity concentrations.

The network-level accessibility is the mean of the node-level values,

$$\text{Accessibility}(G(t)) = \frac{1}{|V|} \sum_{r=1}^{|V|} A_r(t), \tag{13}$$

and the normalized accessibility performance at timestep $t$ is given by

$$P_{\text{Accessibility}}(t) = \frac{\text{Accessibility}(G(t))}{\text{Accessibility}(G)}. \tag{14}$$

As disruptions intensify and paths become longer or unavailable, $P_{\text{Accessibility}}$ decreases accordingly.

### 3.3.3. Local redundancy

Local redundancy captures the availability of short, alternative routes in the immediate vicinity of each intersection, reflecting the redundancy component of the 4R's framework. We quantify it using the number of triangles (closed triads of mutually adjacent nodes) in the underlying undirected representation of the network. In a road network, a triangle corresponds to a small redundant loop that offers an alternative local detour if one link fails; a higher triangle count therefore indicates greater local route redundancy. This measure is monotone non-increasing under link removal, since deleting an edge can only destroy triangles and never create them.

Let $\Delta(G(t))$ denote the number of triangles in the disrupted network $G(t)$. The normalized local-redundancy performance at timestep $t$ is defined relative to the intact network:

$$P_{\text{Redundancy}}(t) = \min\left(1, \frac{\Delta(G(t))}{\Delta(G)}\right). \tag{15}$$

This measure takes values in $[0, 1]$, where 1 indicates that local redundancy is at or above its intact-network level and lower values indicate a loss of alternative local routes.

### 3.3.4. Global connectivity

Global connectivity describes the extent to which nodes remain part of a single functioning network component following disruption. We assess it using the relative size of the largest connected component, which captures network-scale fragmentation rather than local structure.

Let $\text{LCC}(G(t))$ denote the number of nodes in the largest connected component of the disrupted network $G(t)$, and let $|V|$ denote the total number of nodes in the network. Global connectivity is defined as:

$$\text{Connectivity}(G(t)) = \frac{\text{LCC}(G(t))}{|V|}. \tag{16}$$

This measure takes values in $[0, 1]$, where a value of 1 indicates that all nodes belong to a single connected component and lower values indicate increasing network fragmentation. To facilitate comparison across networks and recovery trajectories, the connectivity metric is normalized relative to the undamaged network:

$$P_{\text{Connectivity}}(t) = \frac{\text{Connectivity}(G(t))}{\text{Connectivity}(G)}. \tag{17}$$

### 3.3.5. Spatial fairness

Spatial fairness characterizes how evenly accessibility is distributed across the network during recovery. Building on the node-level accessibility $A_r(t)$ defined in the Accessibility subsection, we quantify spatial inequality using the far component of a spatial Gini decomposition, which emphasizes disparities between geographically distant parts of the network.

To distinguish inequalities occurring over different spatial scales, we construct a distance-based proximity matrix using the Euclidean distances $d_{rs}$ between nodes $v_r$ and $v_s$ in the intact network. The proximity weight between two distinct nodes is defined as:

$$w_{rs} = \begin{cases} \dfrac{1}{(d_{rs} + \epsilon)^b}, & r \neq s, \\ 0, & r = s, \end{cases} \tag{18}$$

where $\epsilon$ is a small constant to avoid division by zero and $b$ is a distance-decay parameter, set to 1.0 in this study. The proximity weights are subsequently normalized to the interval $[0, 1]$.

Let $\overline{A}(t)$ denote the mean accessibility across all nodes,

$$\overline{A}(t) = \frac{1}{|V|} \sum_{r=1}^{|V|} A_r(t). \tag{19}$$

The spatial inequality measure is defined as the far component of the accessibility Gini decomposition,

$$Q(t) = \frac{\sum_{r=1}^{|V|} \sum_{s=1}^{|V|} \left(1 - w_{rs}\right) \left|A_r(t) - A_s(t)\right|}{2|V|^2 \overline{A}(t)}. \tag{20}$$

Finally, the normalized spatial fairness metric is computed by comparing the current spatial inequality with that of the intact network,

$$P_{\text{Fairness}}(t) = 1 - \frac{\max\left(Q(t) - Q(0), 0\right)}{G_{\max} - Q(0)}, \tag{21}$$

where $Q(0)$ is the far-spatial Gini coefficient of the intact network and $G_{\max} = 1$ is the maximum attainable Gini coefficient.

This formulation ensures that $P_{\text{spatial}}(t) \in [0, 1]$, where values close to 1 indicate that accessibility inequalities have not increased relative to the intact network, while progressively lower values indicate increasing spatial concentration of accessibility disadvantages across geographically distant regions of the network. By focusing on the far component of the spatial Gini decomposition, the metric emphasizes regional disparities in accessibility that may emerge during network disruption and recovery.

The resilience metrics adopted in this study are deliberately topology-based and do not incorporate travel demand, origin–destination flows, or congestion dynamics. Consistent demand data are unavailable across cities, and demand-based assignment models are generally calibrated on normal-day travel patterns and equilibrium route choice, assumptions that are least reliable under post-disaster conditions marked by trip suppression, demand changes, and non-equilibrium behavior. Topological metrics instead characterize the structural substrate on which any demand pattern must operate; the results should therefore be interpreted as indicators of structural recovery capacity rather than operational traffic performance.

### 3.4. Simulation experiments

The data used for stress testing are generated using a structured simulation framework in which each road network is subjected to synthetic disruptions, followed by incremental link restoration guided by alternative recovery strategies. At each stage of restoration, recovery performance is evaluated across multiple resilience dimensions. An overview of the simulation workflow is provided in Algorithm 1.

For each road network in the sample, disruptions are first simulated by randomly removing a predefined fraction of links, and the resulting performance is assessed relative to the intact network. Disruption intensity is varied incrementally, ranging from 0% to 100% of failed links, to perform stress testing that is agnostic to the type of hazard. This approach provides a benchmark for evaluating the intrinsic resilience of networks and facilitates consistent comparison across a large and heterogeneous set of cities without focusing on any particular hazard type. To account for randomness in both damage realization and recovery dynamics, each combination of initial damage intensity and restoration strategy is simulated 25 times per network. Random failure models are commonly used in graph-theory based approaches as baseline representations of robustness [64,65], as they encompass a wide range of plausible disruption configurations, including unexpected and compound failures.

Random failures nevertheless assume that link failures are spatially independent, whereas many natural hazards, such as floods, earthquakes, and landslides, tend to produce spatially clustered damage, with failure probabilities shaped by the location and extent of the hazard as well as by local terrain and exposure conditions. To examine whether this abstraction affects our conclusions, we complement the main experiments with a spatially correlated (epicenter-based) disruption model in which link failures cluster around randomly located hazard epicenters with distance-decaying intensity Appendix A. For a representative network, the relative ranking of recovery strategies is preserved under spatially correlated damage across all disruption intensities. Absolute performance losses, on the other hand, are smaller because clustered damage confines its impact to a subregion of the network. By construction, the two damage models converge as the disrupted share approaches 100%. The random-failure stress test, therefore, provides a conservative upper bound of recovery losses under more extreme disruptions without altering the comparative conclusions about recovery strategies, supporting the use of the hazard-agnostic random model for the large-scale analysis.

In the second stage, damaged links are restored sequentially according to the priority order specified by each recovery strategy. After each restoration step, network performance is evaluated along five dimensions, namely, operational efficiency, accessibility,

**Algorithm 1** Simulation workflow for generating the resilience analysis dataset.

**Require:** Set of road networks $G \in \mathbf{G}$, recovery strategies $h \in H$, damage percentages $pct \in \mathcal{P}$, number of replications $N$, restoration batch size $v$
**Ensure:** Dataset for regression modeling
**for** each network $G \in \mathbf{G}$ **do**
  **for** each damage percentage $pct \in \mathcal{P}$ **do**
    **for** $i = 1$ **to** $N$ **do**
      Generate disrupted network $G(0)$ by randomly removing $pct\%$ of links from $G$
      Compute baseline performance metrics on the intact network $G$
      Compute initial performance metrics on the disrupted network $G(0)$
      **for** each recovery strategy $h \in H$ **do**
        Set restoration step counter $t \leftarrow 1$
        Initialize current network as $G(t) \leftarrow G(0)$
        **while** there exist unrestored links **do**
          Rank remaining disrupted links according to priority rule defined by strategy $h$
          Select and restore the top-ranked batch (approximately $v\%$ of total original links)
          Update the list of remaining disrupted links
          Re-compute network performance across resilience dimensions $m \in M$ on the partially restored network $G(t)$
          Store normalized performance values $P_m(t)$ for each dimension $m$
          Increment $t \leftarrow t + 1$
        **end while**
      **end for**
    **end for**
  **end for**
  Collect and store all simulation outcomes for network $G$ across damage levels, replications, and strategies
**end for**
Merge simulation results from all networks into a single dataset
Calculate topology-related variables for every network $G \in \mathbf{G}$
Derive final resilience metrics for each dimension by applying trapezoidal integration over the recovery trajectories
Assemble the complete dataset containing topological features, disruption intensity ($pct$), strategy indicators, and integrated resilience outcomes

local redundancy, global connectivity, and spatial fairness, and recovery trajectories are constructed. We also defined the number of damaged links to be repaired at each time step as a fixed percentage of the total number of links in the network, ensuring that the availability of recovery resources is controlled and does not affect recovery outcomes across cities. Consequently, "time" in the simulations advances in units of restoration steps, and all recovery trajectories are expressed as functions of the cumulative share of restored links. Strategy rankings are similar when the batch size is halved or doubled (for more details, see Appendix B.4). Moreover, expressing the batch size as a fixed percentage of network links holds the relative recovery rate constant across cities by design, so that differences in recovery outcomes reflect network topology and restoration strategy rather than differences in recovery resources. In practice, recovery capacity depends on crew availability, budgets, site accessibility, and repair durations, which vary across cities and events.

These recovery trajectories correspond conceptually to the 4R's framework proposed by [12], in which both performance degradation and restoration over time is captured using the concept of resilience triangle. In the third stage, we aggregated simulated performance curves across all networks, disruption levels, and strategies, and computed the cumulative performance loss in terms of the resilience metrics discussed in Section 3.3 using trapezoidal integration. The resulting resilience metrics are merged with network-level topological characteristics to form a comprehensive dataset.

### 3.5. Statistical analysis and regression modeling

The role of network topology in shaping the effectiveness of recovery strategies is examined through a beta-regression framework [66]. This approach is well suited to the analysis because the recovery performance indicators, $\mathbf{P}_m$, are continuous and restricted to the unit interval. These indicators compute effectiveness of recovery in terms of resilience metrics by measuring the area above the recovery trajectories. Each model treats one of the performance measures introduced in Section 3.3 as the outcome variable.

Model estimation is carried out using a logit link, where the linear predictor $\eta_m$ is expressed as $\eta_m = \ln\left(\mu_m/(1-\mu_m)\right)$, with $\mu_m$ representing the expected value of the standardized performance metric. The regression coefficients $(\beta_{0,m}, \beta_{1,m}, \delta_{r,m}, \gamma_{h,m}, \psi_{h,m})$ describe how recovery performance responds to damage severity, network structure, and recovery policy. Damage severity is captured by the variable $pct$, defined as the share of disrupted links. Network structure enters the model through a set of topological descriptors $x_r$. Recovery strategies are incorporated as categorical variables $\mathbb{I}(h)$, benchmarked against random recovery, while the terms $\psi_{h,m}$ allow the effect of damage to vary across strategies. Because the simulated recovery trajectories are nested within road networks (all trajectories from a given city share its topology, and the topological predictors vary only between cities), the model

residuals cannot be treated as independent across observations. Statistical inference is therefore based on standard errors clustered at the network level [67,68], which are robust to arbitrary correlation among observations from the same network.

$$\eta_m = \beta_{0,m} + \beta_{1,m} pct + \sum_{r \in R} \delta_{r,m} x_r + \sum_{h \in S} \gamma_{h,m} \cdot \mathbb{I}(h) + \sum_{h \in S} \psi_{h,m} \big(\mathbb{I}(h) \cdot pct\big), \tag{22}$$

The explanatory variables included in the model can be grouped into four categories: (i) disruption intensity, captured by *pct*; (ii) structural characteristics of the pre-disruption network; (iii) categorical variables representing the centrality-based recovery strategy employed; and (iv) interaction variables that allow the effectiveness of recovery strategies to vary with the level of initial damage.

The set of topological predictors is drawn from an initial pool of network descriptors representing size, connectivity, redundancy, and spatial configuration. These include the number of road network edges, network density, mean and standard deviation of node degree, global and average clustering coefficients, average link length measured in metres, degree assortativity, and average link travel time measured in minutes.

## 4. Results and discussion

In this subsection, we present the analysis and model results and discuss the major findings and inferences.

### 4.1. Data description

The analysis was performed on a set of 224 real-world road networks (Fig. 3), varying in topological and geographic properties. These networks were randomly selected from 75 countries spanning six continents (Europe: 66 cities, Asia: 39, North America: 32, Africa: 28, Australia/Oceania: 11, and South America: 7), considering a wide variety of urban road network structures, from grid-like structures to irregular networks. Generative artificial intelligence tools were also used to assist in the curation of the final list of networks. All road networks and associated data were obtained from OpenStreetMap. For each road link, directionality is taken from the "oneway" tags in OpenStreetMap as interpreted by the OSMnx package [69]: road segments explicitly tagged as one-way are represented by a single directed arc, while segments without a directionality tag follow the OpenStreetMap default of two-way operation and are represented by a pair of opposing arcs. Across the 224 networks in the sample, 7.9% of road links belong to one-way segments. Although tagging errors or omissions in OpenStreetMap may occasionally misrepresent local directionality, oneway coverage in urban driving networks is generally reliable, and any residual misclassifications default conservatively to two-way operation rather than to spurious one-way restrictions. To manage computational complexity and limit topological variability within networks, only cities with at most 2500 road edges are included. Nevertheless, the sample retains substantial variation in topological characteristics. Table 1 reports the summary statistics of the key topological features considered in this study.

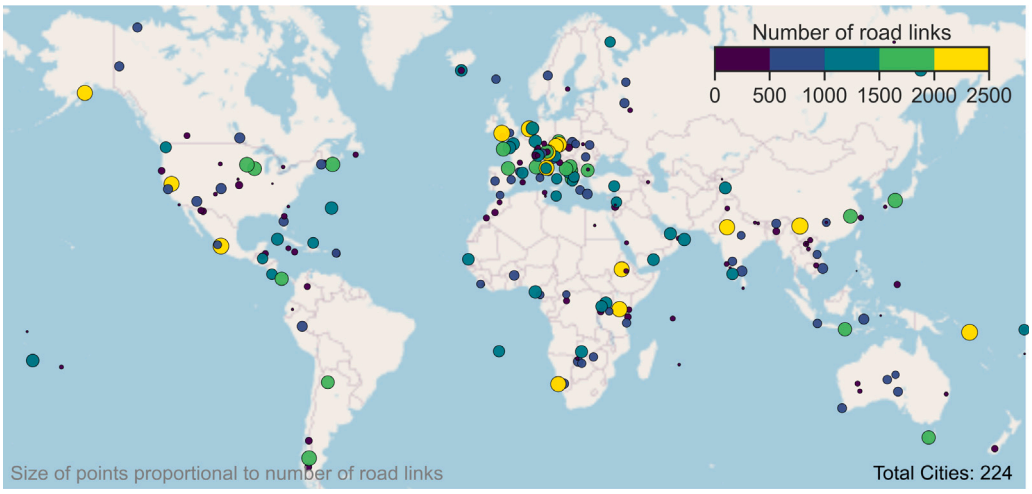



**Fig. 3.** Geographic distribution of the road network sample ($|\mathbf{G}| = 224$).

In total, we attempted 369,600 full network recovery simulations (224 networks × 11 initial failure percentages × 6 recovery strategies × 25 random edge failure combinations) were attempted, of which 356,400 (96.4%) completed and form the final dataset. Each network recovery simulation involved evaluation of performance metrics at multiple stages of recovery as recovery actions were performed incrementally, as shown in Algorithm 1. The performance and resilience metrics were computed for each of the completed recovery simulations. A small percentage of the simulations were not completed due to computational constraints with respect to time and are therefore omitted from the final dataset.

**Table 1**
Summary statistics of selected 224 road networks.

| Topological metric | Mean | Standard deviation | Min | Median | Max |
|---|---|---|---|---|---|
| Number of edges | 799.08 | 637.01 | 14.00 | 657.50 | 2427.00 |
| Density | 0.02 | 0.03 | 0.00 | 0.01 | 0.21 |
| Average degree | 4.83 | 0.60 | 3.10 | 4.77 | 6.50 |
| Degree standard deviation | 1.80 | 0.19 | 1.19 | 1.81 | 2.21 |
| Global clustering coefficient | 0.08 | 0.05 | 0.01 | 0.07 | 0.40 |
| Average clustering coefficient | 0.08 | 0.06 | 0.01 | 0.07 | 0.57 |
| Assortativity (degree) | 0.04 | 0.18 | −0.33 | 0.01 | 0.51 |
| Average link length (m) | 292.52 | 528.42 | 53.45 | 152.03 | 5397.43 |
| Average link travel time (min) | 30.93 | 57.76 | 4.66 | 16.32 | 647.69 |

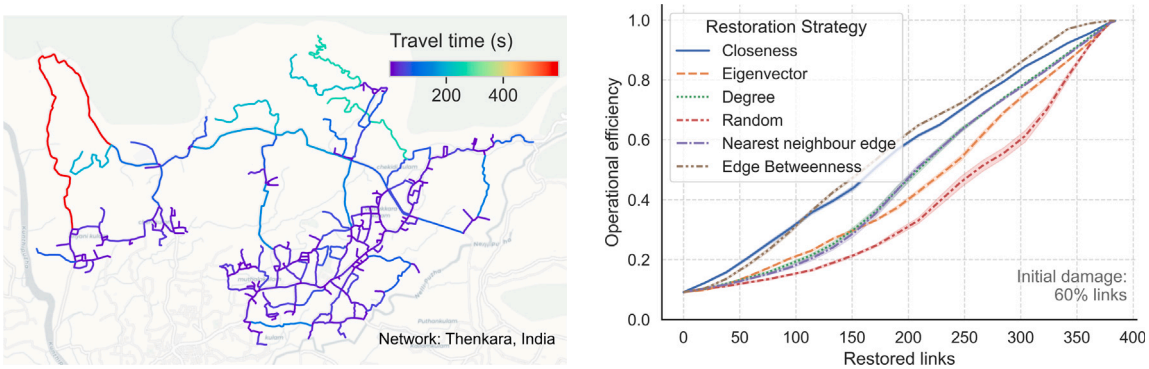
### 4.2. Simulation of road network resilience dataset

All simulations were executed on the DelftBlue supercomputer, hosted by TU Delft [70]. Each simulation run was assigned to a dedicated compute node equipped with 32 Intel Xeon Gold 6226R CPU cores (2.90 GHz, max. 3.90 GHz) and 128 GB of memory (3.9 GB per core). Within the simulation, parallelization was implemented using Python's multiprocessing library, distributing computations associated with road networks to different CPU cores.

### 4.3. Simulation results and statistical modeling

#### 4.3.1. Influence of recovery strategy on different performance metrics

Once the road recovery data were simulated, we analyzed the effectiveness of all recovery strategies across all performance metrics. Fig. 4 shows the effectiveness of the six strategies on the OpenStreetMap road network from Thenkara, India, with 60% of the links initially disrupted. The network is depicted in Fig. 4(a), and the simulated recovery curves for the operational efficiency metric are shown in Fig. 4(b). The results indicate that, for this specific network and performance metric, recovering edges based on their edge betweenness score generally yields superior performance, with strategies based on eigenvector and degree centrality also performing relatively better. While closeness centrality performs moderately well in the early stage of recovery, its performance gradually deteriorates at the later stages of recovery.




(a) Road network topology in Thenkara, India.

(b) Simulated recovery trajectories and confidence intervals.

**Fig. 4.** Simulated recovery curves based on operational efficiency metric under different recovery strategies when initial disruption is 60% of links. Strategies with smaller area above the curve are more effective.

However, these recovery patterns cannot be generalized across networks and performance metrics. Fig. 5 shows the performance loss curves for all five performance metrics and all six recovery strategies for a different road network based in the city of Honiara, Solomon Islands. These results show that strategies do not perform uniformly across disaster intensity and for different performance metrics. For example, when spatial fairness is considered as the resilience metric, closeness centrality-based recovery outperforms the other strategies for most initial damage levels. For connectedness, nearest neighbor edge centrality outperforms the other strategies for most damage levels. Interestingly, certain recovery strategies perform worse than random recovery strategies for certain performance metrics. For example, random recovery tends to lead to better connectivity than recovery based on betweenness centrality. This is intuitive, as random recovery may involve repair actions that are more spatially dispersed, thereby improving connectivity at a faster pace than a betweenness centrality–based strategy.

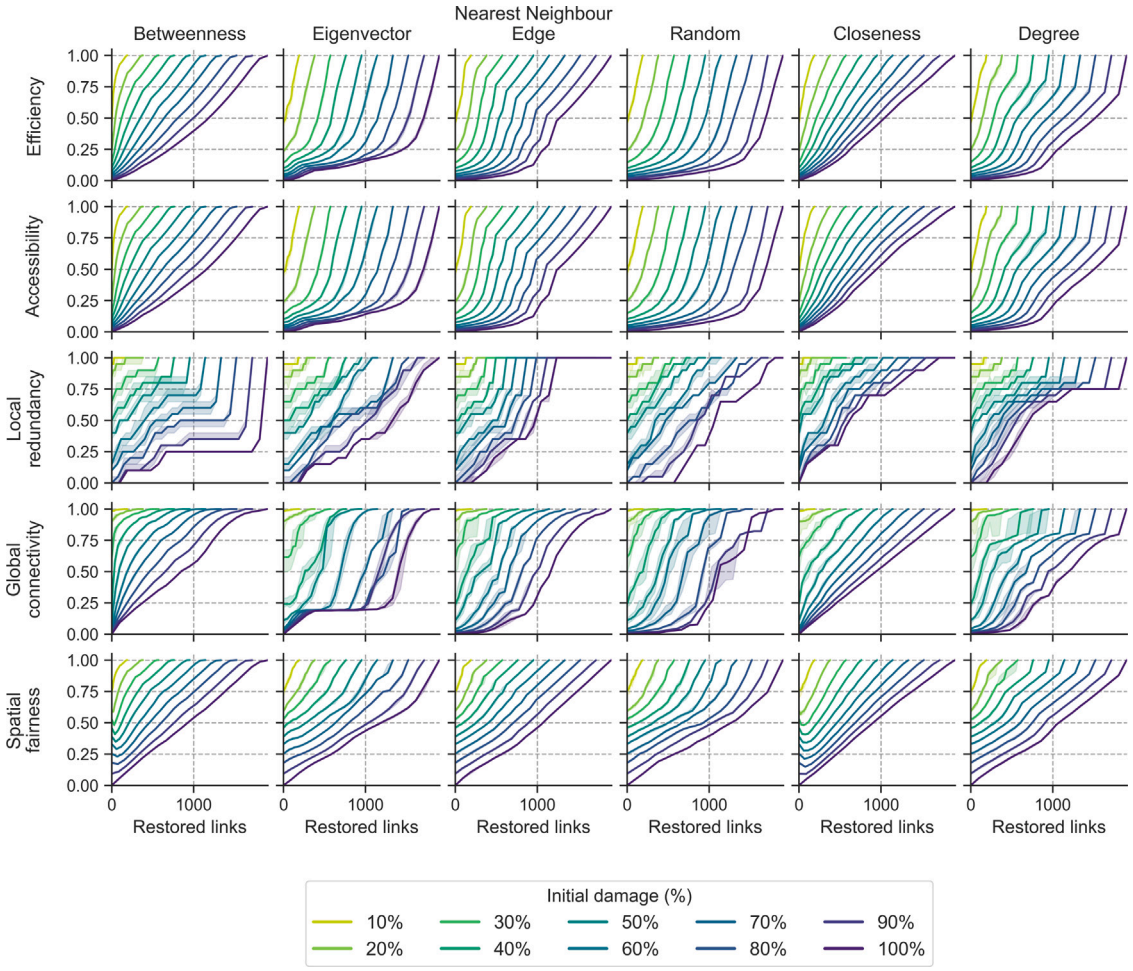



**Fig. 5.** Performance trajectories under the six restoration strategies and 10 damage intensities simulated using the road network in Honiara, Solomon Islands.

*4.3.2. Modeling the association between multidimensional resilience, topological characteristics, and recovery strategies*

To examine the influence of topological design of road networks on the effectiveness of recovery strategies across different resilience dimensions, as well as to identify the best strategy for each dimension, we adopted regression analyses. To avoid collinearity in the regression models, Pearson correlation tests (Fig. 6) were performed, and a recursive pruning algorithm was applied to iteratively remove topological variables with correlations above 0.4. As a result, network-level topological variables, including density, global and average clustering coefficients, assortativity, and average travel time, were excluded, leaving four relatively independent predictors: number of edges, average node degree, standard deviation of node degrees, and average link length. Variance inflation factors (VIFs) computed on the final model dataset confirm the absence of problematic multicollinearity: the four retained topological predictors have VIFs between 1.03 and 1.10, well below conventional thresholds (see Appendix B.2). The moderate VIFs of the strategy indicators and their interaction terms ($5.8 - 6.2$) are structural, arising mechanically from the inclusion of interactions with their own main effects and from the shared categorical origin of the strategy dummies, and do not affect the interpretability of the estimates. These four variables, together with the baseline damage variable (percentage of undisrupted network is chosen due to technical reasons), recovery strategy indicators, and their interactions, form the final predictor set used in the regression analysis. Table 2 presents the results of the beta regression models examining recovery outcomes across five resilience dimensions. All models are estimated on 356,400 observations and demonstrate a strong fit, with precision parameters between 1.53 and 2.62. Likelihood ratio (LR) tests indicated that all fitted beta regression models provided a significantly better fit than their intercept-only counterparts (all $p < 0.001$), confirming that the predictors substantially improved model fit. Because coefficients are on the logit of the mean response (bounded in $[0, 1]$), we interpret signs and magnitudes on the mean scale by back-transforming to predicted values under representative network conditions. Statistical significance is assessed using network-clustered standard errors, which exceed conventional standard errors by factors of roughly 1.5 to 4 for the strategy and interaction terms and 7 to 23 for the topological predictors (see Appendix B.1), reflecting that the effective information content for between-network characteristics derives from 224 distinct networks rather than the independent 356,400 observations. The disruption-intensity,

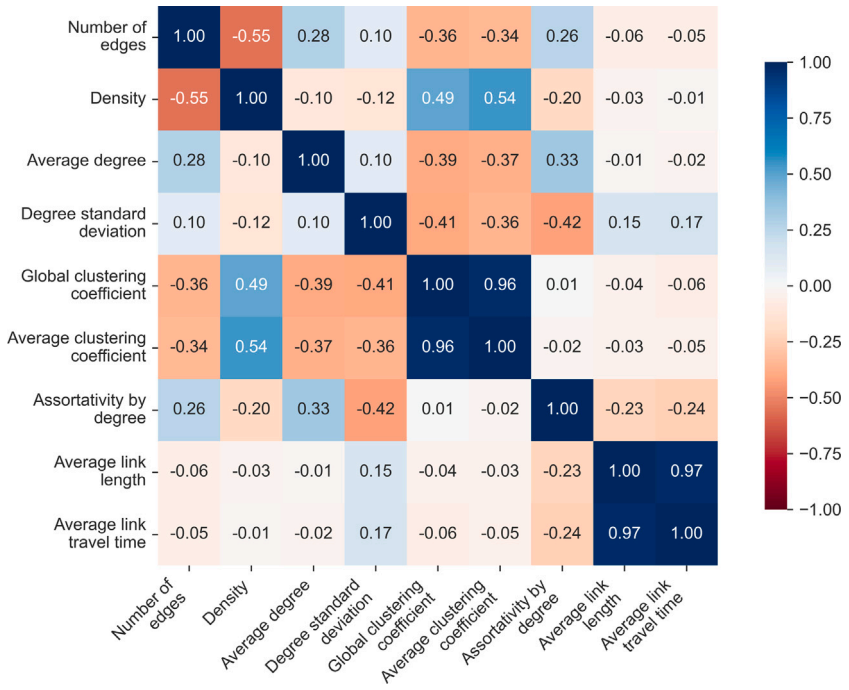



**Fig. 6.** Pearson's correlation coefficients of topological characteristic pairs.

**Table 2**
Beta regression models for resilience quantification based on the five metrics.

| Predictors | Resilience loss models (estimated using beta regression) | | | | |
|---|---|---|---|---|---|
| | Efficiency | Accessibility | Local redundancy | Global connectivity | Spatial fairness |
| Intercept | 2.096‡ | 2.603‡ | 2.509‡ | 1.792‡ | 1.288‡ |
| Undamaged links (%) | −0.043‡ | −0.042‡ | −0.040‡ | −0.048‡ | −0.032‡ |
| *Structural properties of network* | | | | | |
| Network edges | 0.0002‡ | 0.0003‡ | 0.0004‡ | 0.0003‡ | 0.0002† |
| Average degree | −0.158‡ | −0.207‡ | −0.118† | −0.408‡ | −0.253‡ |
| Degree standard deviation | 0.092 | −0.075 | −0.775‡ | 0.231* | 0.096 |
| Average length | −0.00009‡ | −0.00010‡ | −0.00007 | 0.00005 | −0.00004 |
| *Recovery strategy (reference level: Random)* | | | | | |
| Betweenness | −1.071‡ | −1.044‡ | 0.720‡ | −0.549‡ | −0.434‡ |
| Closeness | −0.973‡ | −1.015‡ | −0.265‡ | 0.033 | −0.145‡ |
| Degree | −0.222‡ | −0.106† | −0.022 | 0.274‡ | −0.055* |
| Eigenvector | −0.222‡ | −0.210‡ | 0.065 | 0.135‡ | −0.019 |
| Near-neighbor edge | −0.304‡ | −0.270‡ | −0.072* | 0.283‡ | −0.078† |
| *Interactions: Disruption extent and recovery strategy* | | | | | |
| Undamaged links (%) × Betweenness | 0.008‡ | 0.008‡ | −0.008‡ | 0.006‡ | 0.003‡ |
| Undamaged links (%) × Closeness | 0.009‡ | 0.009‡ | 0.003‡ | 0.002‡ | 0.002‡ |
| Undamaged links (%) × Degree | 0.003‡ | 0.001‡ | 0.001‡ | −0.001‡ | 0.001‡ |
| Undamaged links (%) × Eigenvector | 0.003‡ | 0.003‡ | 0.000 | 0.0004 | 0.000 |
| Undamaged links (%) × Near-neighbor | 0.003‡ | 0.003‡ | 0.002‡ | −0.002‡ | 0.001‡ |
| *Model statistics* | | | | | |
| Precision parameter ($\phi$) | 2.007‡ | 1.843‡ | 1.529‡ | 2.618‡ | 1.811‡ |
| Number of observations | 356,400 | 356,400 | 356,400 | 356,400 | 356,400 |
| Number of networks (clusters) | 224 | 224 | 224 | 224 | 224 |
| Likelihood Ratio | 549,901‡ | 508,541‡ | 457,132‡ | 712,553‡ | 388,496‡ |
| AIC | −765,200 | −724,300 | −1,066,000 | −1,565,000 | −855,600 |

Note: All models use beta regression with maximum likelihood estimation. Significance levels are based on the cluster-robust standard errors and denoted as $^{*}p < 0.05$, $^{\dagger}p < 0.01$, $^{\ddagger}p < 0.001$; coefficients without a superscript are not statistically significant at the 5% level. The dependent variables are cumulative performance loss indicators, with higher values corresponding to worse recovery outcomes. Random recovery serves as the reference category for all strategy indicators. Local redundancy is operationalized using the triangle count of the underlying undirected network, while global connectivity is quantified using the relative size of the largest connected component. A comparison of conventional and cluster-robust standard errors is provided in B.1.

strategy, and interaction effects that underpin the main findings remain highly significant under clustered inference, whereas several smaller topological effects, most notably degree heterogeneity and average link length in some models, are no longer statistically distinguishable from zero; these are noted below and in Table 2. The topological coefficients are also found to be stable under leave-one-out respecification of the covariate set (see Appendix B.3). Throughout, we emphasize substantive magnitudes over statistical significance. The regression results demonstrate that performance loss during recovery is jointly shaped by disruption intensity, network structure, and recovery strategies, with significant variation across the five resilience dimensions. Among these, the extent of initial damage is a dominant predictor of resilience outcomes. The coefficients on the percentage of undamaged links are consistently negative across all models ($\beta = -0.043$ for efficiency loss, $\beta = -0.042$ for accessibility loss, $\beta = -0.040$ for local redundancy loss, $\beta = -0.048$ for global connectivity loss, and $\beta = -0.032$ for spatial fairness loss). This indicates that greater intactness at the start of recovery significantly reduces losses, while more severe damage exacerbates them. For example, let us assume that the expected baseline loss across all resilience metrics is 0.40 for interpretability. A 10 percentage point increase in undamaged links lowers the expected efficiency loss to $\mu' = 0.30$ ($\beta = -0.043 \implies \mu' = \text{logit}^{-1}(\text{logit}(0.40) - 0.043 \times 10)$), a reduction of approximately 24%. If the baseline were higher (e.g., 0.60), the same increase in undamaged links would reduce the expected loss to roughly $\mu' = 0.49$ ($\mu' = \text{logit}^{-1}(\text{logit}(0.60) - 0.043 \times 10)$; 18% reduction). These results suggest that networks with less initial damage are more sensitive to further disruptions, while heavily damaged networks experience proportionally smaller improvements.

Beyond disruption intensity and resilience strategies, structural features of the network also shape recovery trajectories. The number of edges has positive coefficients across all models (e.g., $\beta = 0.0003$ in the accessibility loss model), indicating that larger networks tend to experience higher performance losses. For example, at a baseline accessibility loss of 0.40, an increase of 100 links raises the expected mean loss to about $\mu' = 0.41$ ($\beta = 0.0003$), a 1.8% increase. While the marginal effect per link is negligible, network size becomes a significant determinant of resilience when comparing networks of substantially different sizes, reflecting the complexity of recovery in larger networks. By contrast, the average degree is negatively associated with losses. For efficiency, a one–unit increase in mean degree reduces expected mean loss from 0.40 to about $\mu' = 0.36$ ($\beta = -0.158$), approximately a 9.3% reduction, while in accessibility it lowers losses from 0.40 to $\mu' = 0.35$ ($\beta = -0.207$), a 12.1% reduction. These results highlight the resilience benefits of more densely connected networks. The role of degree heterogeneity (standard deviation of node degree) is more nuanced. Its strongest and most robust effect is on local redundancy, where greater heterogeneity is associated with substantially lower losses ($\beta = -0.775$, $p < 0.001$), and it remains positively associated with global connectivity losses ($\beta = 0.231$, $p < 0.05$): a one-unit increase raises the expected connectivity loss from 0.40 to about $\mu' = 0.46$, a 14.1% increase, indicating that hub-dominated layouts are more prone to fragmentation during recovery. Its apparent associations with efficiency, accessibility, and spatial fairness losses, by contrast, are not statistically distinguishable from zero once within-network dependence is accounted for. Average edge length has substantively small effects that are statistically robust only for efficiency and accessibility (e.g., a 1000 m increase changes efficiency loss from 0.40 to $\mu' = 0.38$, $\beta = -0.00009$, about a 5.3% reduction); its coefficients in the remaining models are not significant under clustered inference and are not interpreted further. Overall, network topology exerts important but mixed influences: more highly connected network structures generally enhance recovery performance, whereas larger network size and greater structural heterogeneity can create vulnerabilities that vary across resilience dimensions. These aspects must be considered in both design and recovery planning. The sensitivity of predicted mean loss values across the five resilience dimensions to changes in disruption- and topology-related predictors is presented in Table 3, which illustrates the scale of these effects under a representative baseline disruption.

The regression results further indicate that the effectiveness of recovery strategies is highly contingent on both the extent of initial disruption and the resilience dimension considered. Fig. 7 illustrates predicted performance losses based on mean network characteristics, highlighting that strategy effects emerge through their interactions with damage levels rather than as constant advantages. The mean performance losses are calculated assuming average values for the topological predictors in the model.

For efficiency loss, prioritizing the restoration of high-betweenness roads (for e.g., the arterials carrying the greatest share of shortest paths) provides substantial benefits under severe disruption: at 0% undamaged links, betweenness reduces mean loss from 0.840 (random recovery) to 0.642, with closeness close behind (0.664), while eigenvector, nearest-neighbor edge, and degree

**Table 3**
Predicted mean loss values ($\mu'$) for changes in predictor values, assuming a baseline mean loss of 0.40.

| Change in predictor values | Updated mean loss values based on change in predictors ($\mu'$) | | | | |
|---|---|---|---|---|---|
| | Efficiency loss | Accessibility loss | Local redundancy loss | Global connectivity loss | Spatial fairness loss |
| Initial undamaged % (+10%) | 0.302 | 0.305 | 0.309 | 0.292 | 0.326 |
| Network edges (+100 edges) | 0.405 | 0.407 | 0.410 | 0.407 | 0.405 |
| Average degree (+1) | 0.363 | 0.351 | 0.372 | 0.307 | 0.341 |
| Degree standard deviation (+1) | 0.422 | 0.382 | 0.235 | 0.456 | 0.423 |
| Average length (+1000 metres) | 0.379 | 0.376 | 0.383 | 0.412 | 0.390 |

Notes: Predictions assume a baseline mean loss of 0.40. Changes represent unit increases in predictors (e.g., +10% undamaged links, +100 edges, +1 degree, +1 degree standard deviation, +1000 m average edge length). $\mu'$ denotes the predicted mean loss after applying the coefficient effect. Column order follows the five resilience dimensions: operational efficiency, accessibility, local redundancy, global connectivity, and spatial fairness. Predicted values are shown for completeness for all predictors; entries based on coefficients that are not statistically significant under network-clustered inference (see Table 2) should be interpreted as indistinguishable from the baseline of 0.40.

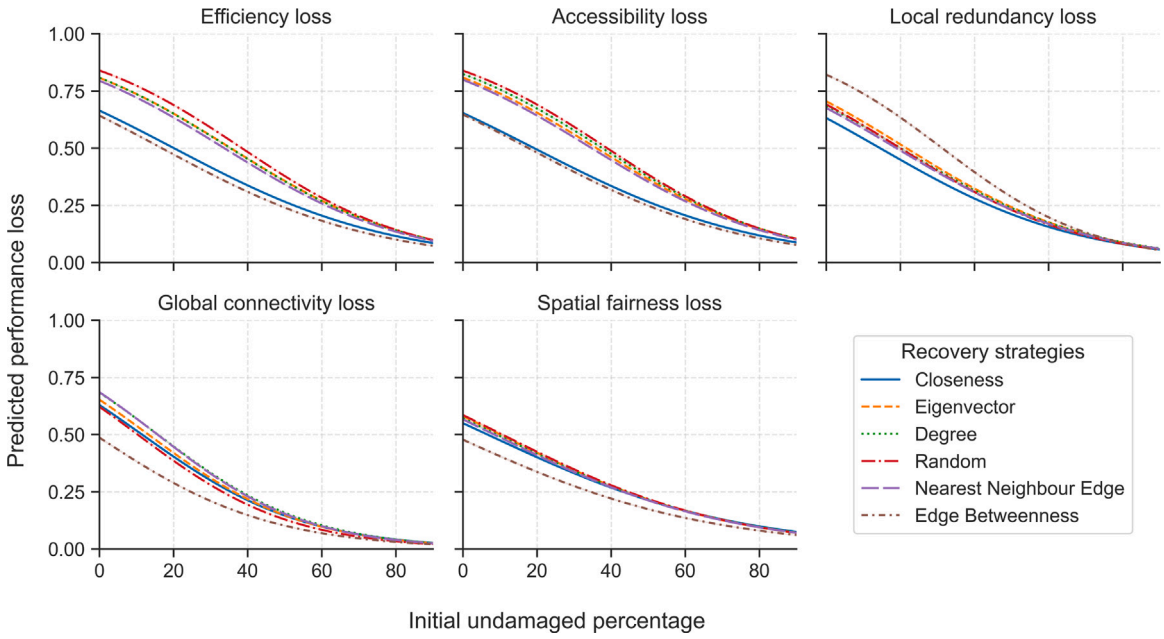



**Fig. 7.** Interaction effects of recovery strategy and damage extent on performance loss metrics. Notes: (a) all predictions based on mean values for network properties of networks considered, (b) predicted performance losses ($\mu_m$) for various initial damage percentages are standardized using corresponding maximum possible loss values.

strategies offer smaller gains. As disruption decreases, strategies converge, with betweenness and closeness maintaining only a slight advantage. Accessibility loss shows a similar pattern: at 0% undamaged (indicating full network damage), restoring central destinations first through betweenness (0.647) and closeness (0.654) outperforms random recovery (0.839) by significant margins, but benefits diminish with higher undamaged percentages. Local redundancy loss, reflecting the availability of short, parallel local detours, reverses this ordering: betweenness performs worst under severe disruption (0.821 versus 0.691 for random recovery), consistent with its negative interaction term, as concentrating repairs on major arterials leaves the minor connecting streets comparatively depleted; closeness is instead the most effective strategy (0.632). For global connectivity loss, which indicates the extent to which the network avoids splitting into isolated districts, betweenness is the most effective strategy under severe disruption (0.487 versus 0.622 for random recovery), while degree and nearest-neighbor strategies perform worst (0.684 and 0.686). Under clustered inference, closeness-based recovery is statistically indistinguishable from random recovery for global connectivity, and eigenvector-based recovery does not differ significantly from random recovery for local redundancy and spatial fairness, indicating that not all centrality heuristics provide benefits on every dimension. Spatial fairness loss, capturing how evenly restored access is distributed across the study area, shows the smallest spread across strategies: betweenness again yields the lowest loss (0.478 versus 0.586 for random recovery), with the remaining strategies clustered closely together.

In summary, three findings emerge from the analysis that have significant policy implications for both infrastructure development and management. Road network resilience is intrinsically multidimensional: no single restoration strategy dominates across all metrics, and the best strategy in one dimension may perform poorly in another, as betweenness-based restoration illustrates by serving global connectivity and spatial fairness well but local redundancy poorly. Network topology also shapes recovery: a higher average number of connections per junction lowers efficiency, accessibility, and connectivity losses, whereas hub-dominated layouts and larger network size tend to increase them. Finally, although graph-based strategies offer little advantage under mild disruptions, they substantially accelerate recovery under large-scale disruptions.

From an engineering perspective, these results highlight the importance of evaluating trade-offs among multiple recovery objectives and tailoring restoration strategies to network topology and disruption intensity.

## 5. Conclusions

Using a dataset of 224 real-world road networks extracted from OpenStreetMap, this study simulated network disruptions and recovery under six semi-operational strategies, evaluated across five performance dimensions, namely network efficiency, accessibility, local redundancy, global connectivity, and spatial fairness. Statistical analysis of the resulting performance trajectories revealed how disruption intensity, network topology, and repair strategies jointly shape recovery outcomes.

The findings demonstrate that road network resilience cannot be captured using one metric. No single recovery strategy delivers consistent benefits across all resilience dimensions. In particular, strategies that improve recovery outcomes from the standpoint of

one dimension (e.g., efficiency) may not be optimal in the case of another dimension (e.g., local redundancy), underscoring the need to evaluate recovery holistically. Pre-disaster robustness, expressed through denser and more connected network structures, generally enhances recovery capacity, although the effects of structural heterogeneity vary across resilience dimensions. Meanwhile, graph-theory-based repair strategies offer limited advantage under minor disruptions but accelerate recovery significantly in large-scale events.

These results highlight the importance of coupling proactive network design with adaptive, context-sensitive recovery planning. Policymakers should therefore adopt a multidimensional approach to resilience, explicitly accounting for trade-offs between resilience dimensions, such as, efficiency, accessibility, local redundancy, global connectivity, and spatial fairness, instead of depending on uniform, generic solutions. Structured methods such as multi-criteria decision analysis could help capture stakeholder priorities and weigh different resilience dimensions. At the same time, investments in robust and redundant infrastructure prior to disasters remain critical. More connected network structures generally enhance resilience, whereas greater structural concentration can create vulnerabilities, particularly for global connectivity. Particularly in disaster-prone regions, deliberate design choices that balance everyday performance with efficient recovery under disruptions are, therefore, needed to ensure that robustness and redundancy at the design stage translate into resilience in practice.

These findings have significant practical implications, particularly in light of the projected US$6.9 trillion in annual investments by 2030 for infrastructure supporting the Sustainable Development Goals (SDGs) and the Paris Agreement [71]. This study demonstrates that network topology and design significantly influence post-disaster recovery, offering actionable insights for resilient infrastructure design. By integrating resilience into the planning phase of critical infrastructure networks, such as power distribution systems, water systems, and communication networks, investors and operators can reduce recovery costs and ensure long-term functionality, particularly in the event of climate-induced extreme events and natural hazards.

At the same time, the study presents several opportunities to improve the results further, as follows:

- The topology-based metrics capture structural recovery capacity but not operational traffic performance. Incorporating demand and congestion dynamics could alter the findings: capacity constraints would penalize strategies that concentrate restored flow onto few high-centrality arterials, potentially narrowing the betweenness advantage under severe disruption, while demand-weighted accessibility could shift the spatial fairness results where population and network centrality diverge. Dynamic traffic assignment for selected case-study cities with available demand data would allow these effects to be quantified.
- The framework assumes homogeneous, proportionally scaled recovery resources; in practice crew availability, budgets, site accessibility, and repair durations vary across cities and events, and incorporating heterogeneous resource constraints is a natural extension.
- For city-specific policies, beyond the stylized random and epicenter-based models considered here, probabilistic hazard-specific scenarios (flood depth maps, ground-motion fields) must be developed to more accurately represent floods, earthquakes, or landslides and thereby produce recovery patterns that reflect real-world conditions.
- Validation with observed post-event recovery data would enable evaluation of transferability and strengthen the correspondence between simulated resilience metrics and operational recovery performance.

Despite further room for improvement considering the above aspects, this study showed that road network resilience is shaped by the interaction of disruption intensity, network structure, and recovery strategies, and that resilience must be understood as a multidimensional concept. Explicitly recognizing trade-offs between efficiency, accessibility, local redundancy, global connectivity, and spatial fairness can guide both the design of more sustainable transport networks and the planning of recovery strategies that are equitable, robust, and adaptive to future hazards.

## CRediT authorship contribution statement

**Srijith Balakrishnan:** Writing – review & editing, Writing – original draft, Visualization, Validation, Supervision, Software, Resources, Project administration, Methodology, Investigation, Formal analysis, Data curation, Conceptualization. **Patrick Stokkink:** Writing – review & editing, Writing – original draft, Validation, Methodology, Investigation, Conceptualization.

## Declaration of Generative AI and AI-assisted technologies in the writing process

During the preparation of this manuscript, the authors used generative AI tools to assist with language editing, proofreading, paraphrasing, and exploring alternative ways to present results (e.g., tables and figure layouts). All AI-generated content was carefully reviewed, verified, and edited by the authors, who take full responsibility for the accuracy, originality, and integrity of the work and confirm that the manuscript reflects their own analysis and scientific contributions.

## Declaration of competing interest

The authors declare that they have no known competing financial interests or personal relationships that could have appeared to influence the work reported in this paper.

## Appendix A. Recovery under spatially correlated disruptions

The main analysis employs uniformly random link failures as a hazard-agnostic stress test, whereas real hazards such as floods, earthquakes, and landslides produce spatially clustered damage. To assess whether the comparative conclusions are sensitive to the spatial distribution of damaged links, we repeat the recovery experiments on the road network of Honiara, Solomon Islands, under an epicenter-based disruption model and compare the outcomes with those under random failures.

In the epicenter model, each disruption scenario begins by placing a hazard epicenter at a location $\mathbf{e}$, sampled uniformly at random from the junction coordinates of the network. The severity of the hazard then decays smoothly with distance from this epicenter, in the way that ground shaking attenuates away from an earthquake source or flood depths recede from an inundation core. Formally, the hazard intensity $\omega_a$ experienced by a road link $a = (v_i, v_j) \in A$ is evaluated at its midpoint $\mathbf{z}_a$ using a Gaussian decay function,

$$\omega_a = \exp\left(-\frac{\|\mathbf{z}_a - \mathbf{e}\|^2}{2\,d_0^2}\right), \qquad d_0 = f\,L, \tag{A.1}$$

where $d_0$ controls the spatial extent of the hazard footprint. Rather than fixing this width in absolute units, it is expressed as a fraction $f$ of the diagonal $L$ of the network's bounding box (here $f = 0.15$), so that the hazard footprint occupies a comparable share of the urban area regardless of whether the city under study is spatially compact or extensive.

To keep the two damage models directly comparable, the epicenter model fails exactly the same number of links as the random model at any given damage percentage $pct$, namely $n_f = \max(1, \mathrm{round}(|A| \cdot pct/100))$; the two models differ only in *which* links fail. The failed links are drawn without replacement, with the probability of failure increasing steeply with local hazard intensity (proportional to $\omega_a^\kappa$, implemented using a Gumbel top-$k$ sampling procedure). The sharpness exponent, set to $\kappa = 8$, concentrates failures strongly within the hazard footprint: at low damage percentages, the failed links form a contiguous "hole" of impassable roads around the epicenter, and as $pct$ increases, the damaged region grows outward, mimicking hazard footprints of increasing severity. A thin fringe of scattered failures away from the epicenter is deliberately retained, reflecting the isolated damage (for example, from debris or localized flooding) that typically accompanies real events beyond the main impact zone.

All other elements of the simulation are identical to the main experiments: the same six recovery strategies, the same restoration batch size, and the same performance evaluation at each restoration step. A fresh epicenter is drawn for each of the 20 disruption realizations per damage level ($pct \in \{20, 60, 80\}\%$), so that the results average over hazard positions rather than reflecting the vulnerability of any particular district. Because the number of failed links and the restoration increments coincide across the two damage models by construction, any difference between the resulting recovery trajectories is attributable solely to the spatial clustering of damage.

Fig. A.8 presents mean recovery trajectories with 95% confidence bands for operational efficiency, accessibility, and spatial fairness under the two damage models. Three observations emerge. First, the relative ranking of recovery strategies is preserved

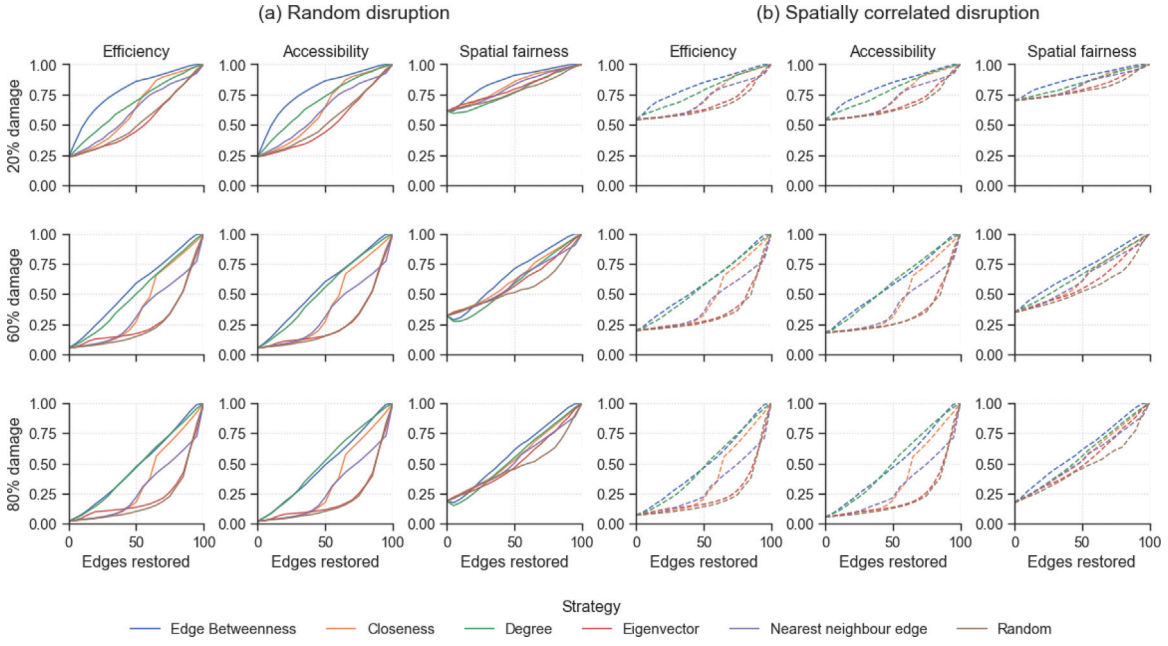



**Fig. A.8.** Recovery trajectories under uniformly random (panel a, solid lines) and spatially correlated epicenter-based (panel b, dashed lines) disruptions for the Honiara road network, across three resilience dimensions (columns) and three initial damage levels (rows). Lines show means over 20 disruption realizations with 95% confidence bands; under the epicenter model a fresh epicenter is sampled per realization.

across damage models at every damage level and dimension shown: strategies that dominate under random failures also dominate under clustered failures, so the comparative conclusions of the main analysis are not artifacts of the uniform-failure assumption. Second, absolute performance losses are consistently smaller under spatially correlated damage. This is an expected consequence of clustering rather than an indication that such hazards are less severe: when the same number of failures is concentrated within a compact footprint, the remainder of the network stays intact and continues to provide short alternative paths, whereas dispersed failures degrade shortest paths throughout the network. The random-failure stress test therefore constitutes a conservative upper bound on network-wide losses for a given damage percentage, although localized hazards may still impose severe losses on the affected subregion, a distributional effect partially reflected in the persistent gap for the spatial fairness dimension. Third, the two damage models converge as damage intensifies: at 80% damage the trajectories are already close, and in the limit of complete failure the models coincide by construction, since the removed link set approaches the full arc set regardless of its spatial arrangement. Spatial correlation of damage is thus most consequential at low-to-moderate disruption intensities. These results support the use of the hazard-agnostic random failure model for the large-scale comparative analysis, while absolute loss estimates for specific hazard types warrant hazard-informed damage models, as noted in Section 5.

## Appendix B. Robustness of statistical models for road network resilience

### *B.1. Cluster-robust standard errors*

The regression dataset contains 356,400 recovery trajectories nested within 224 road networks, and observations from the same network share its topological characteristics and are therefore not independent. Conventional standard errors treat all 356,400 trajectories as independent observations and therefore overstate the precision of the estimates, particularly for the between-network predictors, whose effective sample size is closer to the number of networks than to the number of trajectories. The cluster-robust (sandwich) estimator corrects for this by aggregating the score contributions of all observations within a network before estimating the coefficient covariance, thereby allowing arbitrary correlation and heteroscedasticity within networks while assuming independence only between them [67,68]. The resulting standard errors are valid measures of sampling variability with respect to the population of networks, treating each city, rather than each simulated trajectory, as the fundamental unit of analysis. All inferences reported in Table 2 are therefore based on cluster-robust (sandwich) standard errors with clustering at the network level.

Table B.4 compares conventional and cluster-robust standard errors for the four topological predictors across the five resilience models. Clustered standard errors exceed their conventional counterparts by factors of approximately 7 to 23 for the topological predictors, and by factors of approximately 1.5 to 4 for the strategy indicators and their interactions with disruption extent (not tabulated), confirming substantial within-network dependence. The effects underpinning the main findings are robust to this correction: disruption intensity, the strategy contrasts for efficiency and accessibility, the interaction effects, network size, and average degree remain significant at the 0.1% level in all models. A small number of weaker topological effects do not survive clustered inference at the 5% level: degree standard deviation for efficiency ($p = 0.09$), accessibility ($p = 0.40$), and spatial fairness

**Table B.4**
Conventional versus network-clustered standard errors for the topological predictors.

| Model | Predictor | Conventional Standard Error ($SE$) | Clustered Standard Error ($SE_{clustered}$) | Ratio ($SE_{clustered}/SE$) |
|---|---|---|---|---|
| Efficiency loss | Network edges | 0.000002 | 0.000013 | 6.7 |
| | Average degree | 0.0023 | 0.0192 | 8.2 |
| | Degree standard deviation | 0.0073 | 0.0548 | 7.5 |
| | Average length | 0.000003 | 0.000024 | 7.9 |
| Accessibility loss | Network edges | 0.000003 | 0.000024 | 9.4 |
| | Average degree | 0.0025 | 0.0289 | 11.8 |
| | Degree standard deviation | 0.0077 | 0.0889 | 11.6 |
| | Average length | 0.000003 | 0.000028 | 9.8 |
| Local redundancy loss | Network edges | 0.000003 | 0.000042 | 14.8 |
| | Average degree | 0.0027 | 0.0375 | 13.6 |
| | Degree standard deviation | 0.0086 | 0.1143 | 13.3 |
| | Average length | 0.000005 | 0.000068 | 13.8 |
| Global connectivity loss | Network edges | 0.000002 | 0.000024 | 13.7 |
| | Average degree | 0.0020 | 0.0342 | 16.8 |
| | Degree standard deviation | 0.0064 | 0.0952 | 14.9 |
| | Average length | 0.000003 | 0.000027 | 10.5 |
| Spatial fairness loss | Network edges | 0.000003 | 0.000070 | 23.3 |
| | Average degree | 0.0025 | 0.0429 | 16.9 |
| | Degree standard deviation | 0.0079 | 0.1501 | 18.9 |
| | Average length | 0.000003 | 0.000031 | 10.9 |

($p = 0.52$); average link length for local redundancy ($p = 0.14$), global connectivity ($p = 0.06$), and spatial fairness ($p = 0.20$); the closeness strategy contrast for global connectivity ($p = 0.21$); the degree ($p = 0.48$) and eigenvector ($p = 0.13$) strategy contrasts for local redundancy; and the eigenvector contrast for spatial fairness ($p = 0.42$). The corresponding interpretations in Section 4 are qualified accordingly, while all remaining conclusions are unaffected.

### B.2. Variance inflation factors to check multicollinearity

Variance inflation factors (VIFs) were computed for the final design matrix to evaluate multicollinearity among the predictors, with the results presented in Table B.5.

**Table B.5**
Variance inflation factors for the regression design matrix.

| Predictor | VIF |
|---|---|
| *Structural properties of network* | |
| Network edges | 1.10 |
| Average degree | 1.09 |
| Degree standard deviation | 1.04 |
| Average length | 1.03 |
| *Disruption extent* | |
| Undamaged links (%) | 6.00 |
| *Recovery strategy indicators* | |
| Betweenness, Closeness, Degree, Eigenvector, Near-neighbor edge | 5.84 (each) |
| *Interactions with undamaged links (%)* | |
| All five strategy interactions | 6.17 (each) |

Note: VIFs are computed on the design matrix used in all five beta regression models (the predictor set is identical across models); the intercept is excluded. Identical values within the strategy and interaction groups reflect the balanced experimental design, in which every strategy is applied to every disruption realization. The elevated VIFs for strategy and interaction terms are structural, arising from the inclusion of interaction terms alongside their main effects, and do not indicate collinearity among distinct predictors.

The topological predictors retained after recursive correlation pruning (Section 4.3.2) exhibit VIFs close to 1, indicating that their coefficients are estimated from essentially independent variation. The elevated VIFs of the strategy indicators and interaction terms reflect the mechanical correlation between interactions and their constituent main effects rather than redundancy among distinct predictors, and are therefore not a cause for concern.

### B.3. Model specification stability

As an additional check on specification sensitivity, each of the five models was re-estimated dropping one topological predictor at a time, and the signs of the remaining topological coefficients were compared with the full specification. Across all five resilience dimensions and all leave-one-out specifications, 19 of the 20 topological coefficients retain their sign. The single exception is degree standard deviation in the accessibility model, whose coefficient is statistically indistinguishable from zero under clustered inference (Table 2); sign instability of a null coefficient under respecification is expected and corroborates, rather than contradicts, the clustered-inference result. The topological effects interpreted in Section 4 are therefore stable with respect to both within-network dependence and the choice of covariate set.

### B.4. Recovery batch-size sensitivity

Finally, we assess the sensitivity of the findings to the restoration batch size $\nu$, which the main experiments fix at 5% of network links per restoration step. For a stratified subsample of ten networks spanning the size range of the study sample, the recovery experiments were repeated with the batch size halved ($\nu = 2.5\%$) and doubled ($\nu = 10\%$) at three initial damage levels (20%, 60%, and 80%), holding all other settings identical to the main experiments. For every network, damage level, and resilience dimension, the six recovery strategies were ranked by mean cumulative performance loss, and the agreement of these rankings across batch sizes was quantified using Kendall's rank correlation coefficient $\tau_K$ (Table B.6). Rankings are invariant across batch sizes: mean $\tau_K$ is at least 0.97 for all dimensions and batch-size pairs, and the lowest value observed in any individual network-damage combination ($\tau_K = 0.733$) corresponds to two adjacent strategies exchanging places among the six, never to a reordering of the best- and worst-performing strategies. The comparative conclusions of the main analysis are therefore robust to the assumed restoration batch size.

**Table B.6**
Agreement of strategy rankings across restoration batch sizes (Kendall's $\tau_K$).

| | $\nu = 2.5\%$ vs 5% | | $\nu = 5\%$ vs 10% | | $\nu = 2.5\%$ vs 10% | |
|---|---|---|---|---|---|---|
| Resilience dimension | Mean | Min | Mean | Min | Mean | Min |
| Efficiency | 1.000 | 1.000 | 0.987 | 0.867 | 0.987 | 0.867 |
| Accessibility | 0.996 | 0.867 | 0.991 | 0.867 | 0.996 | 0.867 |
| Local redundancy | 0.991 | 0.867 | 0.978 | 0.867 | 0.969 | 0.733 |
| Global connectivity | 0.996 | 0.867 | 0.991 | 0.867 | 0.987 | 0.867 |
| Spatial fairness | 0.991 | 0.867 | 0.991 | 0.867 | 0.982 | 0.867 |

Note: Strategy rankings computed per network and damage level from mean cumulative performance loss over 20 disruption realizations; means and minima taken over ten networks × three damage levels (20%,60%, 80%). With six strategies, $\tau_K = 0.867$ corresponds to a single adjacent transposition in the ranking and $\tau_K = 0.733$ to two.

## Data availability

The simulation code, processed datasets, and analysis scripts used in this study are publicly accessible at: https://github.com/srijithbalakrishnan/transport_stresstesting. The underlying road network data are publicly available through OpenStreetMap under the Open Database License (ODbL).

## References

[1] J. Jacobo, What to know about the deadly Australia bushfires and why they're expected to continue for months, 2020, URL: https://abcnews.go.com/International/deadly-bushfires-australia-expected-continue-months/story?id=68030661, News Article. ABC News. (Accessed 30 September 2025).
[2] G. Toohey, C. Harter, Canyon fire: Evacuation zones, closures, shelters, 2025, URL: https://www.latimes.com/california/story/2025-08-07/canyon-fire-evacuation-zones-closures-shelters. News Article. Los Angeles Times. (Accessed 30 September 2025).
[3] The Guardian Staff, India floods: At least 15 killed as Delhi records heaviest rain in decades, 2023, URL: https://www.theguardian.com/world/2023/jul/10/india-floods-new-delhi-rain-record-deaths, The Guardian. (Accessed 30 September 2025).
[4] N. Coleman, X. Li, T. Comes, A. Mostafavi, Weaving equity into infrastructure resilience research: A decadal review and future directions, Npj Nat. Hazards 1 (1) (2024) http://dx.doi.org/10.1038/s44304-024-00022-x.
[5] X. Zhang, Y. Lu, J. Wang, Y. Qi, Enhancing highway transportation safety resilience during emergencies: A network-based analysis and assessment, PLoS ONE 19 (7) (2024) e0307233, http://dx.doi.org/10.1371/journal.pone.0307233.
[6] Y. Liu, S. McNeil, J. Hackl, B.T. Adey, Prioritizing transportation network recovery using a resilience measure, Sustain. Resilient Infrastruct. 7 (1) (2022) 70–81.
[7] R. Massobrio, O. Cats, Topological assessment of recoverability in public transport networks, Commun. Phys. 7 (1) (2024) 108.
[8] M.J. Benavidez, A.M. Mortlock, Transport sector recovery: Opportunities to build resilience, 2018, Guidance Note, World Bank Group, URL: https://documents.worldbank.org/en/publication/documents-reports/documentdetail/624471541689229858/transport-sector-recovery-opportunities-to-build-resilience.
[9] R. Francis, B. Bekera, A metric and frameworks for resilience analysis of engineered and infrastructure systems, Reliab. Eng. Syst. Saf. 121 (2014) 90–103.
[10] P.M. Murray-Tuite, A comparison of transportation network resilience under simulated system optimum and user equilibrium conditions, in: Proceedings of the 2006 Winter Simulation Conference, IEEE, 2006, pp. 1398–1405.
[11] M. Ouyang, L. Zhao, Do topological models contribute to decision making on post-disaster electric power system restoration? Chaos: Interdiscip. J. Nonlinear Sci. 24 (4) (2014) http://dx.doi.org/10.1063/1.4898731.
[12] M. Bruneau, S.E. Chang, R.T. Eguchi, G.C. Lee, T.D. O'Rourke, A.M. Reinhorn, M. Shinozuka, K. Tierney, W.A. Wallace, D. von Winterfeldt, A framework to quantitatively assess and enhance the seismic resilience of communities, Earthq. Spectra 19 (4) (2003) 733–752.
[13] J. Liu, M. Zhou, S. Wang, P. Liu, A comparative study of network robustness measures, Front. Comput. Sci. 11 (4) (2017) 568–584.
[14] X. Wang, E. Pournaras, R.E. Kooij, P. Van Mieghem, Improving robustness of complex networks via the effective graph resistance, Eur. Phys. J. B 87 (9) (2014) 221.
[15] Z. He, K. Navneet, W. van Dam, P. Van Mieghem, Robustness assessment of multimodal freight transport networks, Reliab. Eng. Syst. Saf. 207 (2021) 107315.
[16] W. Zhang, N. Wang, C. Nicholson, Resilience-based post-disaster recovery strategies for road-bridge networks, Struct. Infrastruct. Eng. 13 (11) (2017) 1404–1413.
[17] X. Guo, Q. Du, Y. Li, Y. Zhou, Y. Wang, Y. Huang, B. Martinez-Pastor, Cascading failure and recovery of metro–bus double-layer network considering recovery propagation, Transp. Res. Part D: Transp. Environ. 122 (2023) 103861.
[18] Y. Zhou, J. Wang, H. Yang, Resilience of transportation systems: concepts and comprehensive review, IEEE Trans. Intell. Transp. Syst. 20 (12) (2019) 4262–4276.
[19] T.Y. Liao, T.Y. Hu, Y.N. Ko, A resilience optimization model for transportation networks under disasters, Nat. Hazards 93 (1) (2018) 469–489.
[20] L. Chen, E. Miller-Hooks, Resilience: An indicator of recovery capability in intermodal freight transport, Transp. Sci. 46 (1) (2012) 109–123.
[21] A. Kaviani, R.G. Thompson, A. Rajabifard, M. Sarvi, A model for multi-class road network recovery scheduling of regional road networks, Transportation 47 (1) (2020) 109–143.
[22] N.U.I. Hossain, S.A. Fazio, J.M. Lawrence, E.D.S. Gonzalez, R. Jaradat, M.S. Alvarado, Role of systems engineering attributes in enhancing supply chain resilience: Healthcare in context of COVID-19 pandemic, Heliyon 8 (6) (2022).
[23] C. Zamiela, N.U.I. Hossain, R. Jaradat, Enablers of resilience in the healthcare supply chain: A case study of US healthcare industry during COVID-19 pandemic, Res. Transp. Econ. 93 (2022) 101174.
[24] K. Liu, C. Zhai, Y. Dong, Optimal restoration schedules of transportation network considering resilience, Struct. Infrastruct. Eng. 17 (8) (2020) 1141–1154, http://dx.doi.org/10.1080/15732479.2020.1801764.
[25] N. Wang, K.F. Yuen, Resilience assessment of waterway transportation systems: Combining system performance and recovery cost, Reliab. Eng. Syst. Saf. 226 (2022) 108673.

[26] M. Arabi, S. Gerasimidis, C. Barchers, J. Oke, Resilience in multilayer transportation infrastructure networks: A review and conceptual framework for equity-based assessment, Sustain. Resilient Infrastruct. 9 (6) (2024) 616–639.
[27] M. Zamanifar, T. Hartmann, Decision attributes for disaster recovery planning of transportation networks; A case study, Transp. Res. Part D: Transp. Environ. 93 (2021) 102771.
[28] Z. Luo, B. Yang, Towards resilient and smart urban road networks: Connectivity restoration via community structure, Sustain. Cities Soc. 75 (2021) 103344.
[29] S. Balakrishnan, L. Jin, B. Cassottana, A. Costa, G. Sansavini, Developing resilience pathways for interdependent infrastructure networks: A simulation-based approach with consideration to risk preferences of decision-makers, Sustain. Cities Soc. 115 (2024) 105795.
[30] E.D. Vugrin, M.A. Turnquist, N.J. Brown, Optimal recovery sequencing for enhanced resilience and service restoration in transportation networks, Int. J. Crit. Infrastructures 10 (3–4) (2014) 218–246.
[31] U. Bhatia, L. Sela, A.R. Ganguly, Hybrid method of recovery: Combining topology and optimization for transportation systems, J. Infrastruct. Syst. 26 (3) (2020) 04020024.
[32] A. Ulusan, O. Ergun, Restoration of services in disrupted infrastructure systems: A network science approach, PLoS One 13 (2) (2018) e0192272.
[33] T. Zhao, Y. Zhang, Transportation infrastructure restoration optimization considering mobility and accessibility in resilience measures, Transp. Res. Part C: Emerg. Technol. 117 (2020) 102700.
[34] S. Moghtadernejad, B.T. Adey, J. Hackl, Prioritizing road network restorative interventions using a discrete particle swarm optimization, J. Infrastruct. Syst. 28 (4) (2022) 04022039.
[35] X. Mao, J. Zhou, C. Yuan, D. Liu, Resilience-based optimization of postdisaster restoration strategy for road networks, J. Adv. Transp. 2021 (1) (2021) 8871876.
[36] J. Lin, Q. Hu, W. Lin, M. Tan, Risk and resilience-based restoration optimization of transportation infrastructures under uncertainty, PLoS One 19 (8) (2024) e0308138.
[37] N.Y. Aydin, H.S. Duzgun, H.R. Heinimann, F. Wenzel, K.R. Gnyawali, Framework for improving the resilience and recovery of transportation networks under geohazard risks, Int. J. Disaster Risk Reduct. 31 (2018) 832–843.
[38] Q. Feng, Q. Wu, X. Hai, Y. Ren, C. Wen, Z. Wang, Deep reinforcement learning-based resilience optimization for infrastructure networks restoration with multiple crews, Front. Eng. Manag. 12 (1) (2025) 141–153.
[39] P. Ghannad, Y.C. Lee, J.O. Choi, Prioritizing postdisaster recovery of transportation infrastructure systems using multiagent reinforcement learning, J. Manag. Eng. 37 (1) (2021) 04020100.
[40] N. Zhang, A. Alipour, L. Coronel, Application of novel recovery techniques to enhance the resilience of transportation networks, Transp. Res. Rec.: J. Transp. Res. Board 2672 (1) (2018) 138–147.
[41] F. Rouhana, D. Jawad, Transportation network resilience against failures: GIS-based assessment of network topology role, Int. J. Disaster Resil. Built Environ. 12 (4) (2020) 357–370, http://dx.doi.org/10.1108/ijdrbe-06-2020-0064.
[42] C. Gomez, J. Baker, D. Castiblanco, M. Faber, Coupled pre-and post-disaster decisions in the context of infrastructure resilience, in: International Forum on Engineering Decision Making; Eight Forum: Decision Making beyond the Engineering Comunity, 2015, pp. 1–8.
[43] L.C. Freeman, et al., Centrality in social networks: Conceptual clarification, Soc. Netw.: Crit. Concepts Sociol. 1 (3) (2002) 238–263.
[44] J. Zhang, Y. Luo, Degree centrality, betweenness centrality, and closeness centrality in social network, in: 2017 2nd International Conference on Modelling, Simulation and Applied Mathematics, MSAM2017, Atlantis Press, 2017, pp. 300–303.
[45] D. Koschützki, F. Schreiber, Comparison of centralities for biological networks, in: German Conference on Bioinformatics 2004, GCB 2004, Gesellschaft für Informatik eV, 2004, pp. 199–206.
[46] E. Estrada, Generalized walks-based centrality measures for complex biological networks, J. Theoret. Biol. 263 (4) (2010) 556–565.
[47] M.O. Jackson, et al., Social and economic networks, vol. 3, Princeton university press Princeton, 2008.
[48] P. Bartesaghi, M. Benzi, G.P. Clemente, R. Grassi, E. Estrada, Risk-dependent centrality in economic and financial networks, SIAM J. Financial Math. 11 (2) (2020) 526–565.
[49] J. Wang, H. Mo, F. Wang, F. Jin, Exploring the network structure and nodal centrality of China's air transport network: A complex network approach, J. Transp. Geogr. 19 (4) (2011) 712–721.
[50] S. Derrible, Network centrality of metro systems, PLoS One 7 (7) (2012) e40575.
[51] Y. Zhang, X. Wang, P. Zeng, X. Chen, Centrality characteristics of road network patterns of traffic analysis zones, Transp. Res. Rec.: J. Transp. Res. Board 2256 (1) (2011) 16–24.
[52] K. Das, S. Samanta, M. Pal, Study on centrality measures in social networks: A survey, Soc. Netw. Anal. Min. 8 (2018) 1–11.
[53] A. Landherr, B. Friedl, J. Heidemann, A critical review of centrality measures in social networks, Bus. Inf. Syst. Eng. 2 (2010) 371–385.
[54] I. Stamos, Transportation networks in the face of climate change adaptation: A review of centrality measures, Futur. Transp. 3 (3) (2023) 878–900.
[55] OpenStreetMap, OpenStreetMap, 2025, URL: https://www.openstreetmap.org. (Accessed 01 July 2025).
[56] G. Csardi, T. Nepusz, The igraph software package for complex network research, Complex Systems 1695 (2006) 1–9, URL: https://igraph.org.
[57] Q.V. Guo, J. Lu, Z. Li, Equitable Restoration Strategies for Bridge and Road Infrastructure Networks after Hurricanes in Coastal Communities, Final Report ABC-UTC-2016-C6-FIU04, Florida State University, Department of Civil and Environmental Engineering, Tallahassee, FL, 2024, URL: https://abc-utc.fiu.edu/wp-content/uploads/2025/01/ABC-UTC-Report-QG-FSU.pdf. Sponsored by USDOT Accelerated Bridge Construction University Transportation Center.
[58] N. Yadav, S. Chatterjee, A.R. Ganguly, Resilience of urban transport network-of-networks under intense flood hazards exacerbated by targeted attacks, Sci. Rep. 10 (1) (2020) 10350.
[59] L.C. Freeman, A set of measures of centrality based on betweenness, Sociometry 40 (1) (1977) 35–41, URL: http://www.jstor.org/stable/3033543.
[60] T. Bröhl, K. Lehnertz, A straightforward edge centrality concept derived from generalizing degree and strength, Sci. Rep. 12 (1) (2022) 4407.
[61] P. Bonacich, Factoring and weighting approaches to status scores and clique identification, J. Math. Sociol. 2 (1) (1972) 113–120.
[62] P. Bonacich, Power and centrality: A family of measures, Am. J. Sociol. 92 (5) (1987) 1170–1182.
[63] S. Porta, E. Strano, V. Iacoviello, R. Messora, V. Latora, A. Cardillo, F. Wang, S. Scellato, Street centrality and densities of retail and services in Bologna, Italy, Environ. Plan. B: Plan. Des. 36 (3) (2009) 450–465.
[64] S. Dong, A. Mostafizi, H. Wang, J. Gao, X. Li, Measuring the topological robustness of transportation networks to disaster-induced failures: A percolation approach, J. Infrastruct. Syst. 26 (2) (2020) 04020009.
[65] O. Artime, M. Grassia, M. De Domenico, J.P. Gleeson, H.A. Makse, G. Mangioni, M. Perc, F. Radicchi, Robustness and resilience of complex networks, Nat. Rev. Phys. 6 (2) (2024) 114–131.
[66] S. Ferrari, F. Cribari-Neto, Beta regression for modelling rates and proportions, J. Appl. Stat. 31 (7) (2004) 799–815.
[67] K.Y. Liang, S.L. Zeger, Longitudinal data analysis using generalized linear models, Biometrika (1986) 13–22.
[68] A.C. Colin, D.L. Miller, A practitioner's guide to cluster-robust inference, J. Hum. Resour. 50 (2) (2015) 317–372.
[69] G. Boeing, OSMnx: New methods for acquiring, constructing, analyzing, and visualizing complex street networks, Comput. Environ. Urban Syst. 65 (2017) 126–139.
[70] Delft High Performance Computing Centre, DelftBlue supercomputer (phase 2), 2024, https://www.tudelft.nl/dhpc/ark:/44463/DelftBluePhase2.
[71] OECD, Infrastructure for a climate-resilient future, 2024, http://dx.doi.org/10.1787/a74a45b0-en, OECD Publishing, Paris. ISBN 978-92-64-42194-3 (print). ISBN 978-92-64-76213-8 (PDF). ISBN 978-92-64-31547-1 (HTML). ISBN 978-92-64-69864-2 (epub).